Title 40 CFR Part 191
Subparts B and C
Compliance Recertification Application 2019
for the
Waste Isolation Pilot Plant

Appendix MASS-2019
Performance Assessment
Modeling Assumptions

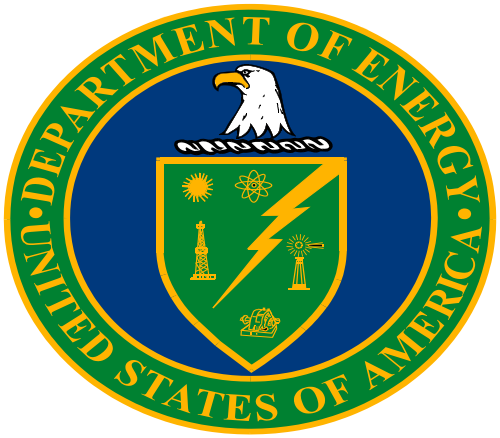

United States Department of Energy
Waste Isolation Pilot Plant

Carlsbad Field Office
Carlsbad, New Mexico

Compliance Recertification Application 2019
Appendix MASS

Table of Contents

List of Tables

List of Figures

Acronyms and Abbreviations

An	actinide
CCA	Compliance Certification Application
CCDF	complementary cumulative distribution function
CFR	Code of Federal Regulations
CH-TRU	contact-handled transuranic
cm	centimeters
CPR	cellulosic, plastic, and rubber
CRA	Compliance Recertification Application
DBR	direct brine release
DOE	U.S. Department of Energy
DRZ	disturbed rock zone
EXP	experimental area/region
EPA	U.S. Environmental Protection Agency
FEP	feature, event, and process
ft	foot
in.	inch
K_d	Culebra matrix partition coefficient
LHS	Latin hypercube sample
m	meter
MB	marker bed
MPa	megapascals
NROR	north rest of repository
OPS	operations area/region
PA	performance assessment
PABC	Performance Assessment Baseline Calculation
PAVT	Performance Assessment Verification Test
pH	measure of the acidity or alkalinity of a solution
RH-TRU	remote-handled transuranic
ROMPCS	Run-of-Mine Panel Closure System
ROR	rest of repository
SROR	south rest of repository
T field	transmissivity field

TRU	transuranic
WIPP	Waste Isolation Pilot Plant
WP	waste panel region of BRAGFLO model

Elements and Chemical Compounds

Am	americium
$CaCO_3$	calcite
CH_4	methane
Cm	curium
CO_2	carbon dioxide
H_2	hydrogen
H_2S	hydrogen sulfide
$Mg(OH)_2$	brucite, magnesium hydroxide
$Mg_5(CO_3)_4(OH)_2 \cdot 4H_2O$	hydromagnesite
MgO	magnesium oxide
Np	neptunium
$PbCO_3$	cerrusite
Pu	plutonium
Th	thorium
U	uranium

This page intentionally left blank.

MASS-1.0 Introduction

This appendix presents supplementary information regarding the assumptions, simplifications, and approximations used in models that underlay the 2019 Compliance Recertification Application (CRA-2019) performance assessment (PA) of the Waste Isolation Pilot Plant (WIPP). The PA executed in support of the fourth WIPP recertification is denoted as the CRA-2019 PA. Within this appendix, relevant issues in the formulation or development of the various types of models (for example, conceptual, mathematical, numerical, or computer code) used for the topic under consideration in each section are discussed, and references to relevant historical information are included where appropriate. This appendix references the Compliance Certification Application (CCA) (U.S. DOE 1996), the 2004 Compliance Recertification Application (CRA-2004) (U.S. DOE 2004), the 2009 Compliance Recertification Application (CRA-2009) (U.S. DOE 2009), and the 2014 Compliance Recertification Application (CRA-2014) (U.S. DOE 2014) when the information discussed has not changed from past demonstrations of compliance with the U.S. Environmental Protection Agency's (EPA's) disposal standards. Historical development of the WIPP conceptual models that led to the PA used in the CCA is documented in the CCA, Appendix MASS, Section MASS-2.0. Historical development of the modeling assumptions for the CRA-2004 PA is documented in Appendix PA-2004, Attachment MASS. Historical development of modeling assumptions used in the CRA-2009 PA is documented in Appendix MASS-2009. Finally, historical development of modeling assumptions used in the CRA-2014 PA is documented in Appendix MASS-2014.

The technical baseline for the first WIPP recertification included modifications required by the EPA during its review of the CRA-2004 PA (Cotsworth 2005). These modifications resulted in a PA called the Performance Assessment Baseline Calculation (PABC), which was denoted as the CRA-2004 PABC. The PA executed in support of the second recertification, the CRA-2009 PA, included a number of technical changes and corrections, as well as updates to parameters and improvements to the PA computer codes (Clayton et al. 2008). To incorporate additional information received after the CRA-2009 PA was completed but before the submittal of the CRA-2009, the EPA requested an additional PA be undertaken, referred to as the CRA-2009 PABC (Clayton et al. 2010), which included updated information (Cotsworth 2009). The PA executed in support of the third recertification, the CRA-2014 PA, included a number of technical changes and corrections, as well as parameter updates (Camphouse et al. 2013).

Several changes are incorporated in the CRA-2019 PA relative to the CRA-2014. The modifications included in the CRA-2019 PA include parameter updates and refinements to PA implementation. A summary of changes in PA since the CRA-2014 is given in the CRA-2019 Appendix PA. Section MASS-2.0 includes a discussion of general modeling assumptions applicable to the disposal system as a whole, including a table of assumptions made in PA models, with cross-references. The remainder of this appendix discusses assumptions specific to the conceptual models used in the CRA-2019 PA.

MASS-2.0 General Assumptions in PA Models

A number of assumptions are applied generally to the disposal system through the conceptual and mathematical models implemented in the CRA-2019 PA. Table MASS-1, which lists modeling assumptions used in the PA, is a guide to general modeling assumptions. Because many of the assumptions in that table have not changed from earlier CRA submittals, material submitted with those recertification applications is listed for reference. References to documents included in the CRA-2019 are also included where appropriate. Table MASS-1 provides guidance for integrating the assumptions with (1) the chapters, sections, or appendices in which they are discussed, and (2) the codes that implement them. The codes are: BRAGFLO (brine and gas flow in and around the Salado formation, as well as direct brine release (DBR) volume calculation), MODFLOW-2000 (brine flow in the Culebra formation), SECOTP2D (radionuclide transport in the Culebra formation), DRSPALL (spallings releases), PEST (parameter estimation), SANTOS (creep closure calculation), NUTS (radionuclide transport in and around the Salado formation), PANEL (radionuclide concentrations), CUTTINGS_S (cuttings and cavings volumes), and CCDFGF (stochastic future calculation and complementary cumulative distribution function [CCDF] assembly).

The features, events, and processes (FEPs) discussed in Appendix SCR-2019 that are relevant to these assumptions are also indicated. The final column in the table indicates whether the U.S. Department of Energy (DOE) considers each assumption to be reasonable or conservative. The DOE has not attempted to bias the overall results of PA toward a conservative outcome. However, the DOE has chosen to use conservative assumptions where data or models are impractical to obtain, or where effects on performance are not expected to be significant enough to justify development of a more complicated model. In all other cases, best unbiased conceptual models and parameter values have been selected. The designator R (reasonable) in the final column indicates that the DOE considers the assumption to be reasonable based on WIPP-specific data or information, data or information considered analogous to the WIPP disposal system, expert judgment, or other reasoning. The designator C (conservative) indicates that the DOE considers the assumption (i.e. model inputs) may overestimate a process or effect.[1] The regulatory designator (Reg) indicates that the assumption is based on regulations in 40 Code of Federal Regulations (CFR) Part 191, criteria in 40 CFR Part 194, or other regulatory guidance.

[1] Conservatism in model inputs may result in lower or higher releases.

Table MASS-1. General Modeling Assumptions

Chapter or Section	Assumption Number	Code	Modeling Assumption	Related FEP in Appendix SCR-2019	Assumption Considered[a]
CRA-2019: MASS-2.0 General Assumptions in PA Models CRA-2019: MASS-2.1 Darcy's Law Applied for Fluid Flow calculated by BRAGFLO, MODFLOW-2000, and DRSPALL	1	BRAGFLO MODFLOW-2000	Flow is governed by mass conservation and Darcy's Law in porous media. Flow is laminar and fluids are Newtonian.	Saturated Groundwater Flow (N23) Unsaturated Groundwater Flow (N24) Brine Inflow (W40)	R
	2	BRAGFLO	Two-phase flow in the porous media is by simultaneous immiscible displacement.	Fluid Flow Due to Gas Production (W42)	R
	3	BRAGFLO	The Brooks-Corey or Van Genuchten/Parker equations represent interactions between brine and gas.	Fluid Flow Due to Gas Production (W42)	R
	4	BRAGFLO	The Klinkenberg effect is included for flow of gases at low pressures.	Fluid Flow Due to Gas Production (W42)	R
	5	BRAGFLO	Threshold displacement pressure for flow of gas into brine is constant.	Fluid Flow Due to Gas Production (W42)	R
	6	BRAGFLO MODFLOW-2000 SECOTP2D	Fluid composition and compressibility are constant.	Saturated Groundwater Flow (N23) Fluid Flow Due to Gas Production (W42)	R
CRA-2019: MASS-2.2 Hydrogen Gas as Surrogate for Waste-Generated Gas Physical Properties in BRAGFLO and DRSPALL	7	BRAGFLO DRSPALL	The gas phase is assigned the density and viscosity properties of hydrogen.	Fluid Flow Due to Gas Production (W42)	R-C

Chapter or Section	Assumption Number	Code	Modeling Assumption	Related FEP in Appendix SCR-2019	Assumption Considered[a]
CRA-2019: MASS-2.3 Salado Brine as Surrogate for Liquid Phase Physical Properties in BRAGFLO	8	BRAGFLO	All liquid physical properties are assigned the properties of Salado brine.	Saturated Groundwater Flow (N23)	R
CRA-2004: 6.4.2 Model Geometries CRA-2004: 6.4.2.1 Disposal System Geometry CRA-2019: MASS-3.0 Model Geometries CRA-2019: MASS-3.1 Disposal System Geometry as Modeled in BRAGFLO	9	BRAGFLO	The disposal system is represented by a two-dimensional, north-south, vertical cross section.	Stratigraphy (N1) Physiography (N39)	R
	10	BRAGFLO	Flow in the disposal system is radially convergent or divergent centered on the repository, shaft, and borehole for disturbed performance.	Saturated Groundwater Flow (N23) Unsaturated Groundwater Flow (N24)	R
	11	BRAGFLO	Variable dip in the Salado is approximated by a one-degree dip to the south.	Stratigraphy (N1)	R
	12	BRAGFLO	Stratigraphic layers are parallel.	Stratigraphy (N1)	R
	13	BRAGFLO	The stratigraphy consists of units above the Dewey Lake, the Forty-niner, the Magenta, the Tamarisk, the Culebra, the Los Medaños, and the Salado Formations (comprising impure halite, marker bed (MB) 138, anhydrites A and B [lumped together], and MB 139). The dimensions of these units are constant. A Castile brine reservoir is included in the BRAGFLO grid in all scenarios.	Stratigraphy (N1)	R
CRA-2004: 6.4.2.2 Culebra Geometry	14	MODFLOW-2000 SECOTP2D	The Culebra is represented by a two-dimensional, horizontal geometry for groundwater flow and radionuclide transport simulation.	Stratigraphy (N1)	R
	15	MODFLOW 2000 PEST	Transmissivity varies spatially. There is no vertical flow to or from the Culebra.	Groundwater Recharge (N54) Groundwater Discharge (N53)	R

Chapter or Section	Assumption Number	Code	Modeling Assumption	Related FEP in Appendix SCR-2019	Assumption Considered[a]
	16	SECOTP2D	The regional flow field provides boundary conditions for local transport calculations (see CRA-2004, Chapter 6.0, Section 6.4.10.2).	Advection (W90)	R
CRA-2004: 6.4.3 The Repository CRA-2019: MASS-3.1 BRAGFLO Geometry of the Repository CRA-2019: MASS-14.0 Intrusion Borehole	17	BRAGFLO	The repository comprises five regions separated by panel closure areas: the waste panel (WP), a north rest of repository (NROR), a south ROR (SROR), an operations (OPS) region, and an experimental (EXP) region (**Figure MASS-1**). The SROR and NROR regions are separated by an intact panel closure, Run-of-Mine Panel Closure System (ROMPCS), while the WP and SROR regions are separated by an open panel closure area that has properties identical to the OPS and EXP regions. The NROR and OPS regions are separated by an intact panel closure (ROMPCS) with length twice the length of the other ROMPCS representation because it also represents a set of panel closures between the OPS and EXP regions. A single shaft region is also modeled, and a borehole region is included for a borehole that intersects the separate WP. The dimensions of these regions are constant.	Disposal Geometry (W1)	R-C
	18	BRAGFLO	Although there will be no waste emplacement in Panel 9, waste is modeled in Panel 9 (see Zeitler et al. 2017 and MASS-14.0).	Disposal Geometry (W1)	C
	19	BRAGFLO	Long-term flow up plugged and abandoned boreholes modeled as if all intrusions occur into a downdip (southern) panel.	Disposal Geometry (W1)	C
	20	BRAGFLO	For each repository region, the model geometry preserves design volume.	Disposal Geometry (W1)	R

Chapter or Section	Assumption Number	Code	Modeling Assumption	Related FEP in Appendix SCR-2019	Assumption Considered[a]
	21	BRAGFLO	Pillars, individual drifts, and rooms are not modeled for long-term performance, and containers provide no barrier to fluid flow.	Disposal Geometry (W1)	C
	22	BRAGFLO	Long-term flow is radial to and from the borehole that intersects the waste disposal panel during disturbed performance.	Waste-Induced Borehole Flow (H32)	R
	23	BRAGFLO	Disturbed rock zone (DRZ) provides a pathway to MBs.	None	R
	24	BRAGFLO	Grid dimensions for the intact and open panel closure areas are consistent with the ROMPCS panel closure design. Material properties for intact panel closure areas are consistent with the ROMPCS panel closure design, while material properties of open panel closure areas are identical to properties in the OPS and EXP regions. Ventilation bulkheads and concrete block walls are assumed to have no long-term impact.	None	R
CRA-2004: 6.4.3.1 Creep Closure CRA-2019: MASS-4.0 Creep Closure CRA-2014: PORSURF	25	SANTOS	Creep closure is modeled using a two-dimensional model of a single room. Mechanical interactions between adjacent rooms in a panel are insignificant.	Salt Creep (W20) Changes in the Stress Field (W21) Excavation-Induced Changes in Stress (W19)	R
	26	SANTOS	The amount of creep closure is a function of time, gas pressure, mechanical properties of the host rock, and waste-matrix strength.	Salt Creep (W20) Changes in the Stress Field (W21) Consolidation of Waste (W32) Pressurization (W26)	R

Chapter or Section	Assumption Number	Code	Modeling Assumption	Related FEP in Appendix SCR-2019	Assumption Considered[a]
	27	BRAGFLO	Porosity of waste areas (WP, SROR, and NROR) is a function of time and brine pressure, which are correlated to time and gas pressure in SANTOS calculations.	Salt Creep (W20)	R
	28	BRAGFLO	Porosity of the open panel closure, OPS and EXP areas is fixed at a value representative of consolidated material.	Salt Creep (W20)	R
CRA-2004: 6.4.3.2 Repository Fluid Flow CRA-2019: MASS-5.0 Repository Fluid Flow	29	BRAGFLO	General assumptions 1 to 8.	None	R for assumptions 1-6 and 8; R-C for assumption 7
	30	BRAGFLO	The waste disposal region is assigned a constant permeability representative of average consolidated waste without backfill.	Saturated Groundwater Flow (N23) Unsaturated Groundwater Flow (N24)	R
CRA-2019: MASS-5.1 Flow Interactions with the Creep Closure Model	31	BRAGFLO	The EXP and OPS regions are assigned a constant permeability representative of unconsolidated material and a constant porosity representative of consolidated material. The open panel closure area between the WP and SROR regions is assigned the same properties as the EXP and OPS regions.	Saturated Groundwater Flow (N23) Unsaturated Groundwater Flow (N24) Salt Creep (N20)	C
CRA-2019: MASS-5.2 Flow Interactions with the Gas Generation Model	32	BRAGFLO	For iron corrosion and microbial degradation associated gas generation (and water production) calculations, the effects of wicking are accounted for by assuming that brine in the repository contacts waste to an extent greater than that calculated by the Darcy Flow model.	Wicking (W41)	R

Chapter or Section	Assumption Number	Code	Modeling Assumption	Related FEP in Appendix SCR-2019	Assumption Considered[a]
CRA-2004: 6.4.3.3 Gas Generation Appendix TRU WASTE-2004 CRA-2019: MASS-6.0 Gas Generation CRA-2019: MASS-6.1 Addition of Radiolysis to Gas Generation Modeling for CRA-2019 CRA-2019: GEOCHEM-3.2 WIPP Chemical Conditions Process Models	33	BRAGFLO	Gas generation occurs by anoxic corrosion of steel containers and Fe and Fe-base alloys in the waste, giving H_2, and by microbial consumption of cellulosics and, possibly, plastics and rubbers (CPR), giving mainly CO_2 and hydrogen sulfide (H_2S). Lead corrosion does not contribute to gas generation (Appendix SCR-2019, Section 6.1.3.2.3). Radiolysis also contributes to gas generation through consumption of brine and production of H_2. Radiolysis of CPR, oxic reactions, and other gas generation mechanisms are insignificant. Gas generation is calculated using the average-stoichiometry model and is dependent on brine availability.	Container Material Inventory (W5) Waste Inventory (W2) Degradation of Organic Material (W44) Gases from Metal Corrosion (W49) Radiolysis (W52)	R-C
	34	BRAGFLO	The anoxic corrosion rate is dependent on liquid saturation. Anoxic corrosion of steel continues until all the zero-valent iron is consumed. Steel corrosion will not be passivated by microbially generated gases (CO_2 or H_2S). The water in brine is consumed by the corrosion reaction.	Brine Inflow (W40) Gases from Metal Corrosion (W49) Degradation of Organic Material (W44)	R
	35	BRAGFLO	Laboratory-scale experimental measurements of gas generation rates at expected room temperatures are used to account for the effects of biofilms and chemical reactions.	Effects of Biofilms on Microbial Gas Generation (W48) Effects of Temperature on Microbial Gas Generation (W45) Chemical Effects of Corrosion (W51)	R

Chapter or Section	Assumption Number	Code	Modeling Assumption	Related FEP in Appendix SCR-2019	Assumption Considered[a]
	36	BRAGFLO	The rate of microbial gas production is dependent on the amount of liquid present. Microbial activity occurs in all the simulations. In 75% of the simulations, microbes may consume all of the cellulosics but none of the plastics and rubbers. In the remaining 25% of the simulations, microbes may consume all of the cellulosics and all of the plastics and rubbers. Microbial production will continue until all biodegradable CPR materials are consumed if brine is present. The MgO backfill will react with the CO_2 and remove it sufficiently from the gaseous phase that the contribution to overall gas generation rates is negligible—the very low amount of CO_2 assumed to exist in the repository does not contribute to the amount of gas generated in the repository.	Brine Inflow (W40) Degradation of Organic Material (W44) Waste Inventory (W2)	C
	37	BRAGFLO	Radiolysis of brine will result in the production of hydrogen and oxygen containing aqueous species such that one mole of gas (H_2) is produced for each net mole of water consumed (Day 2019).	Radiolysis (W52)	R
	38	BRAGFLO	Gas generation due to radiolysis of brine from radionuclides in solution and in wetted-solid form is assumed to contribute to repository pressure (Day 2019).	Radiolysis (W52)	R
	39	BRAGFLO	Only a portion of the disintegration energy associated with wetted-solid alpha-emitting radionuclides in the inventory will contribute to radiolytic H_2 generation (Day 2019).	Radiolysis (W52)	R

Chapter or Section	Assumption Number	Code	Modeling Assumption	Related FEP in Appendix SCR-2019	Assumption Considered[a]
	40	BRAGFLO	The total radiolytic H_2 generation rate (and brine consumption rate) is due to contributions from one or more decaying radionuclides in the waste volume (Day 2019).	Radiolysis (W52)	R
	41	BRAGFLO	Gas dissolution in brine is of negligible consequence.	Fluid Flow Due to Gas Production (W42)	C
	42	BRAGFLO	The gaseous phase is assigned the properties of hydrogen (General Assumption 7).	Fluid Flow Due to Gas Production (W42)	R-C
CRA-2004: 6.4.3.4 Chemical Conditions in the Repository CRA-2019: SOTERM-2.0 Conceptual Framework of Chemical Conditions CRA-2019: MASS-7.0 Chemical Conditions CRA-2019: GEOCHEM-3.0 CRA-2019: SOTERM-6.6	43	NUTS PANEL	Chemical conditions in the repository will be constant. Chemical equilibrium is assumed for all reactions that occur between brine in the repository, waste, and abundant minerals, with the exceptions of gas generation and actinide (An) redox reactions. The uncertainty in redox reaction kinetics (i.e., equilibrium) is taken into account via the source term model where a range of redox conditions is considered across realizations.	Speciation (W56) Reduction-Oxidation Kinetics (W66)	R
	44	NUTS PANEL	Brine and waste in the repository will contain a uniform mixture of dissolved and colloidal species. All An have instant access to all repository brine.	Heterogeneity of Waste Forms (W3) Speciation (W56)	C
	45	NUTS PANEL	No microenvironments that influence the overall chemical environment will persist.	Speciation (W56)	R
	46	NUTS PANEL	For the undisturbed performance and E2 scenarios, brine in the waste regions has the composition of Salado brine. For E1 and E1E2 (Appendix PA-2019, Section PA-2.3.2.2) scenarios, all brine in the waste regions has the composition of Castile brine.	Speciation (W56)	R

Chapter or Section	Assumption Number	Code	Modeling Assumption	Related FEP in Appendix SCR-2019	Assumption Considered[a]
	47	NUTS PANEL	Chemical conditions in the waste panels will be reducing. However, a condition of redox disequilibrium will exist between the possible oxidation states of the An elements.	Reduction-Oxidation Kinetics (W66) Speciation (W56) Effects of Metal Corrosion (W64)	R
	48	NUTS PANEL	The pH and CO_2 fugacity in the waste panels will be controlled by the formation of brucite, hydromagnesite, calcite, and cerrusite. (A result of this assumption is low CO_2 fugacity and mildly basic conditions.)	Speciation (W56) Backfill Chemical Composition (W10)	R
CRA-2004: 6.4.3.5 Dissolved Actinide Source Term	49	NUTS PANEL	Radionuclide dissolution to solubility/inventory limits is instantaneous.	Dissolution of Waste (W58)	C
CRA-2019: GEOCHEM-3.2 The EQ3/6 Computer Code CRA-2019: MASS-8.0 Dissolved Actinide Source Term CRA-2019: Appendix PA-4.4 CRA-2019: SOTERM-6.1	50	NUTS PANEL	Six An (thorium [Th], uranium [U], neptunium [Np], plutonium [Pu], americium [Am], and curium [Cm]) are used in PANEL for calculations of radionuclide transport of brine (up a borehole). Four An (Th, U, Pu, and Am) are explicitly considered in NUTS for calculations of radionuclide transport in brine (porous materials) (Kicker 2019).	Waste Inventory (W2)	R

Chapter or Section	Assumption Number	Code	Modeling Assumption	Related FEP in Appendix SCR-2019	Assumption Considered[a]
	51	NUTS PANEL	The reducing conditions in the repository will eliminate significant concentrations of Np(VI), Pu(V), Pu(VI), and Am(V) species. Am and Cm will exist predominantly in the III oxidation state; while Th will exist in the IV oxidation state. It is assumed that the solubilities and Culebra matrix partition coefficient (K_d) values of U, Np, and Pu will be dominated by one of the remaining oxidation states: U(IV) or U(VI), Np(IV) or Np(V), and Pu(III) or Pu(IV) (See Appendix PA-2019, Section 4.9).	Speciation (W56) Reduction-Oxidation Kinetics (W66)	R
	52	NUTS PANEL	For a given oxidation state, the different An have similar solubilities.	Speciation (W56)	R-C
	53	NUTS PANEL	For undisturbed performance and for all aspects of disturbed performance, except for cuttings and cavings releases (see Assumption 131), radionuclides in the waste are distributed evenly throughout the disposal panel.	Waste Inventory (W2) Heterogeneity of Waste Forms (W3)	R
	54	NUTS PANEL	Mobilization of An in the gas phase is negligible.	Dissolution of Waste (W58)	R

Chapter or Section	Assumption Number	Code	Modeling Assumption	Related FEP in Appendix SCR-2019	Assumption Considered[a]
	55	NUTS PANEL	The inventory limitation for An masses is based on the inventory available in five panels, because, due to the lack of an intact panel closure between the WP and SROR regions, an intrusion into the WP has the potential to provide brine for mobilization of An in both the WP and SROR regions, which correspond to a total of five panels. The inventory limitation applies globally for any panel. Even though the NROR panels are separated by panel closures such that there is no communication expected, the assumption of solubility accounting for up to 5 panels of waste is used.	Dissolution of Waste (W58)	C
	56	NUTS PANEL	An concentrations in the repository will be inventory limited when the mass of an An becomes depleted such that the predicted concentrations cannot be achieved.	Dissolution of Waste (W58)	R
CRA-2004: 6.4.3.6 Source Term for Colloidal Actinides CRA-2019: MASS-9.0 Colloidal Actinide Source Term CRA-2019: SOTERM-3.5	57	NUTS PANEL	Four types of colloids constitute the source term for colloidal An: intrinsic, mineral fragment, microbial, and humic.	Colloid Formation and Stability (W79) Humic and Fulvic Acids (W70)	R
	58	NUTS PANEL	Intrinsic colloids for all An are experimentally defined (Reed, Swanson, and Stanley 2019).	Colloid Formation and Stability (W79)	R
	59	NUTS PANEL	Concentrations of intrinsic colloids and mineral-fragment colloids are modeled as constants derived from experimental data. For humic and microbial colloidal contributions, An concentrations are modeled as proportional to dissolved An concentrations.	Colloid Formation and Stability (W79)	R-C

Chapter or Section	Assumption Number	Code	Modeling Assumption	Related FEP in Appendix SCR-2019	Assumption Considered[a]
	60	NUTS PANEL	In calculating mobilized radionuclide concentrations, the maximum concentration of each An associated with each colloid type is constant.	Actinide Sorption (W61)	R
CRA-2004: 6.4.4 Shafts and Shaft Seals CRA-2019: MASS-10.0 Shafts and Shaft Seals	61	BRAGFLO	General Assumptions 1 to 8.	None	R for assumptions 1-6 and 8; R-C for assumption 7
	62	BRAGFLO	The five shafts connecting the repository to the surface are represented by a single shaft with a cross-section and volume equal to the total volume of the five real shafts and separated from the waste by less than the distance of the nearest real shaft.	Disposal Geometry (W1)	R
	63	BRAGFLO	The shaft seal system is represented by an upper and lower shaft region representing a composite of the actual materials in those regions.	Shaft Seal Geometry (W6) Shaft Seal Physical Properties (W7)	R
	64	BRAGFLO	The shaft is surrounded by a DRZ which heals with time. The DRZ is represented through the composite permeabilities of the shaft system itself, rather than as a discrete zone. The effective permeabilities of shaft materials are adjusted at 200 years after closure to reflect consolidation and possible degradation. Permeabilities are constant for the shaft seal materials through the Rustler formation.	Salt Creep (W20) Consolidation of Shaft Seals (W36) DRZ (W18) Microbial Growth on Concrete (W76) Chemical Degradation of Shaft Seals (W74) Mechanical Degradation of Shaft Seals (W37)	R
	65	NUTS	Radionuclides are not retarded by the seals.	Actinide Sorption (W61) Speciation (W56)	C

Chapter or Section	Assumption Number	Code	Modeling Assumption	Related FEP in Appendix SCR-2019	Assumption Considered[a]
CRA-2004: 6.4.5 The Salado CRA-2019: MASS-11.0 Salado	66	BRAGFLO	General Assumptions 1 to 8.	None	R for assumptions 1-6 and 8; R-C for assumption 7
CRA-2004: 6.4.5.1 Impure Halite CRA-2019: MASS-11.1 High Threshold Pressure for Halite-Rich Salado Rock Units	67	BRAGFLO	Intact rock and hydrologic properties are constant.	Stratigraphy (N1)	R
CRA-2004: 6.4.5.2 Salado Interbeds CRA-2019: MASS-11.2 The Fracture Model	68	BRAGFLO	Interbeds have a fracture-initiation pressure above which local fracturing and changes in porosity and permeability occur in response to changes in pore pressure. A power function relates the permeability increase to the porosity increase. A pressure is specified above which porosity and permeability do not change.	Disruption Due to Gas Effects (W25)	R
	69	BRAGFLO	Interbeds have identical physical properties; they differ only in position, thickness, and some fracture parameters.	Saturated Groundwater Flow (N23)	R
CRA-2004: 6.4.5.3 Disturbed Rock Zone CRA-2019: MASS-11.3 Flow in the DRZ	70	BRAGFLO	The permeability of the DRZ is sampled with the low value similar to intact halite and the high value representing a fractured material. The DRZ porosity is equal to the porosity of Salado halite plus 0.29%.	Disturbed Rock Zone (DRZ) (W18) Roof Falls (W22) Gas Explosions (W27) Seismic Activity (N12) Underground Boreholes (W39)	C-R

Chapter or Section	Assumption Number	Code	Modeling Assumption	Related FEP in Appendix SCR-2019	Assumption Considered[a]
CRA-2004: 6.4.5.4 Actinide Transport in the Salado CRA-2019: MASS-11.4 Actinide Transport in the Salado	71	NUTS	Dissolved An and colloidal An are transported by advection in the Salado. Diffusion and dispersion are assumed negligible.	Advection (W90) Diffusion (W91) Matrix Diffusion (W92)	R
	72	NUTS	Sorption of An in the anhydrite interbeds, colloid retardation, colloid transport at higher than average velocities, coprecipitation of minerals containing An, channeled flow, and viscous fingering are not modeled.	Actinide Sorption (W61) Colloid Transport (W78) Colloid Filtration (W80) Colloid Sorption (W81) Fluid Flow Due to Gas Production (W42) Fracture Flow (N25)	R-C
	73	NUTS	Radionuclides having similar decay and transport properties have been grouped together for transport calculations (Kicker 2019). See also assumptions for dissolved An source term.	Radionuclide Decay and Ingrowth (W12)	R
	74	NUTS	Sorption of An in the borehole is not modeled.	Actinide Sorption (W61)	C
CRA-2004: 6.4.6 Units Above the Salado CRA-2019: MASS-12.0 Geologic Units above the Salado	75	SECOTP2D	Above the Salado, lateral An transport to the accessible environment can occur only through the Culebra.	Saturated Groundwater Flow (N23) Unsaturated Groundwater Flow (N24) Solute Transport (W77)	R
CRA-2004: 6.4.6.1 Los Medaños	76	MODFLOW-2000 BRAGFLO	The Los Medaños member of the Rustler Formation, Tamarisk, and Forty-niner are assumed to be impermeable.	Saturated Groundwater Flow (N23)	C

Chapter or Section	Assumption Number	Code	Modeling Assumption	Related FEP in Appendix SCR-2019	Assumption Considered[a]
CRA-2004: 6.4.6.2 The Culebra CRA-2019: MASS-13.0 Flow through the Culebra CRA-2014: TFIELD CRA-2019: MASS-15.0 Climate Change	77	MODFLOW-2000 SECOTP2D	General Assumptions 1, 6, and 8.	None	R
	78	MODFLOW-2000	For fluid flow, the Culebra is modeled as a uniform (single-porosity) porous medium.	Saturated Groundwater flow (N23)	R
	79	MODFLOW-2000	The Culebra flow field is determined from the observed hydraulic conditions and estimates of the effects of climate change and potash mining outside the controlled area and does not change with time unless mining is predicted to occur in the disposal system in the future.	Saturated Groundwater Flow (N23) Climate Change (N61) Precipitation (e.g., Rainfall) (N59) Temperature (N60) Changes in Groundwater Flow Due to Mining (H37)	R
	80	BRAGFLO	The Culebra is assigned a single permeability to calculate brine flow into the unit from an intrusion borehole.	Natural Borehole Fluid Flow (H31) Waste-Induced Borehole Flow (H32)	R
	81	MODFLOW-2000	Gas flow in the Culebra is not modeled. Gas from the repository does not affect fluid flow in the Culebra.	Saturated Groundwater Flow (N23) Fluid Flow Due to Gas Production (W42)	R
	82	BRAGFLO MODFLOW-2000 SECOTP2D	Different thicknesses of the Culebra are assumed for BRAGFLO, MODFLOW-2000, and SECOTP2D calculations, although the transmissivities are consistent.	Effects of Preferential Pathways (N27)	R

Chapter or Section	Assumption Number	Code	Modeling Assumption	Related FEP in Appendix SCR-2019	Assumption Considered[a]
	83	PEST	Uncertainty in the spatial variability of the Culebra transmissivity is accounted for by statistically generating 100 transmissivity fields (T fields) for PA.	Saturated Groundwater Flow (N23) Fracture Flow (N25) Shallow Dissolution (N16)	R
	84	MODFLOW-2000 BRAGFLO	Potentiometric heads are set on the edges of the regional grid to represent flow in a portion of a much larger hydrologic system.	Groundwater Recharge (N54) Groundwater Discharge (N53) Changes in Groundwater Recharge and Discharge (N56) Infiltration (N55)	R
CRA-2004: 6.4.6.2.1 Transport of Dissolved Actinides in the Culebra CRA-2019: MASS-13.1 Dissolved Actinide Transport and Retardation in the Culebra	85	SECOTP2D	Dissolved An are transported by advection in high-permeability features and by diffusion in low-permeability features.	Solute Transport (W77) Advection (W90) Diffusion (W91) Matrix Diffusion (W92)	R
	86	SECOTP2D	Sorption occurs on dolomite in the matrix. Sorption on clays present in the Culebra is not modeled.	Actinide Sorption (W61) Changes in Sorptive Surfaces (W63)	C
	87	SECOTP2D	Sorption is represented using a linear isotherm model.	Actinide Sorption (W61) Kinetics of Sorption (W62)	R

Chapter or Section	Assumption Number	Code	Modeling Assumption	Related FEP in Appendix SCR-2019	Assumption Considered[a]
	88	SECOTP2D	The possible effects on sorption of the injection of brines from the Castile and Salado into the Culebra are accounted for in the distribution of An K_d values.	Actinide Sorption (W61) Groundwater Geochemistry (N33) Changes in Groundwater Eh (N36) Changes in Groundwater pH (N37) Natural Borehole Fluid Flow (H31)	R
	89	SECOTP2D	Hydraulically significant fractures are assumed to be present everywhere in the Culebra.	Advection (W90)	C
CRA-2004: 6.4.6.2.2 Transport of Colloidal Actinides in the Culebra CRA-2019: MASS-13.2 Colloidal Actinide Transport and Retardation in the Culebra	90	SECOTP2D	An humic colloids are chemically retarded identically to dissolved An and are treated as dissolved An.	Advection (W90) Diffusion (W91) Colloid Transport (W78) Microbial Transport (W87)	R
	91	SECOTP2D	The concentration of intrinsic colloids is sufficiently low to justify elimination from PA transport calculations in the Culebra.	None	R
	92	SECOTP2D	Microbial colloids and mineral fragments are too large to undergo matrix diffusion. Filtration of these colloids, which is modeled using an exponential decay approach, occurs in high-permeability features. Attenuation is so effective that associated An are assumed to be retained within the disposal system and are not transported.	Microbial Transport (W87) Colloid Sorption (W81)	R

Chapter or Section	Assumption Number	Code	Modeling Assumption	Related FEP in Appendix SCR-2019	Assumption Considered[a]
CRA-2004: 6.4.6.2.3 Subsidence Due to Potash Mining CRA-2019: MASS-13.3 Subsidence Caused by Potash Mining in the Culebra	93	MODFLOW-2000	The effect of potash mining is to increase the hydraulic conductivity in the Culebra by a factor between 1 and 1,000.	Conventional Underground Potash Mining (H13) Changes in Groundwater Flow Due to Mining (H37)	Reg.
CRA-2004: 6.4.6.3 The Tamarisk	94	MODFLOW-2000 BRAGFLO	The Tamarisk is assumed to be impermeable.	Saturated Groundwater Flow (N23)	R
CRA-2004: 6.4.6.4 The Magenta	95	BRAGFLO	General Assumptions 1 to 8.	None	R for assumptions 1-6 and 8; R-C for assumption 7
	96	BRAGFLO	The Magenta permeability is set to the lowest value measured near the center of the WIPP site. This increases the flow into the Culebra.	Saturated Groundwater Flow (N23)	R
	97	NUTS	No radionuclides entering the Magenta will reach the accessible environment. However, the volumes of brine and An entering and stored in the Magenta are modeled.	Solute Transport (W77)	R
CRA-2004: 6.4.6.5 The Forty-niner	98	BRAGFLO	The Forty-niner is assumed to be impermeable.	Saturated Groundwater Flow (N23)	R
CRA-2004: 6.4.6.6 Dewey Lake	99	BRAGFLO	General Assumptions 1 to 8.	None	R for assumptions 1-6 and 8; R-C for assumption 7
	100	NUTS	The sorptive capacity of the Dewey Lake is sufficiently large to prevent any release over 10,000 years.	Saturated Groundwater Flow (N23) Actinide Sorption (W61)	R
CRA-2004: 6.4.6.7 Supra-Dewey Lake Units	101	BRAGFLO	General Assumptions 1 to 8.	None	R for assumptions 1-6 and 8; R-C for assumption 7

Chapter or Section	Assumption Number	Code	Modeling Assumption	Related FEP in Appendix SCR-2019	Assumption Considered[a]
	102	BRAGFLO	The units above the Dewey Lake are a single hydrostratigraphic unit.	Stratigraphy (N1)	R
	103	BRAGFLO	The units are thin and predominantly unsaturated.	Unsaturated Groundwater Flow (N24) Saturated Groundwater Flow (N23)	R
CRA-2004: 6.4.7 The Intrusion Borehole CRA-2004: 6.4.7.1 Releases during Drilling CRA-2019: MASS-14.0 Intrusion Borehole	104	CUTTINGS_S BRAGFLO DRSPALL	Any An that enter the borehole during drilling are assumed to reach the surface.	None	C
CRA-2019: MASS-14.1 Cuttings, Cavings, and Spall Releases during Drilling	105	BRAGFLO PANEL CUTTINGS_S DRSPALL CCDFGF	Future drilling practices will be the same as they are at present.	Oil and Gas Exploration (H1) Potash Exploration (H2) Oil and Gas Exploitation (H4) Other Resources (H8) Enhanced Oil and Gas Recovery (H9)	Reg.
	106	CUTTINGS_S DRSPALL	Releases of particulate waste material are modeled (cuttings, cavings, and spallings). Releases are corrected for radioactive decay until the time of intrusion.	Drilling Fluid Flow (H21) Suspension of Particles (W82) Cuttings (W84) Cavings (W85) Spallings (W86)	R
	107	CUTTINGS_S	Degraded waste properties are based on surrogate materials.	Cavings (W85)	C

Chapter or Section	Assumption Number	Code	Modeling Assumption	Related FEP in Appendix SCR-2019	Assumption Considered[a]
	108	DRSPALL	A hemispherical geometry with one-dimensional spherical symmetry defines the flow field and cavity in the waste.	Spallings (W86)	C
	109	DRSPALL	Tensile strength based on completely degraded waste surrogates represents extreme, low-end tensile strengths because it does not account for several strengthening mechanisms.	Spallings (W86)	C
	110	DRSPALL	Shape factor is 0.1, corresponding to particles that are easier to fluidize and entrain in the flow.	Spallings (W86)	C
CRA-2004: 6.4.7.1.1 Direct Brine Release During Drilling CRA-2019: MASS-14.2 Direct Brine Releases during Drilling	111	BRAGFLO PANEL	Brine containing An may flow to the surface during drilling. DBR will have negligible effect on the long-term pressure and saturation in the WP region.	Blowouts (H23)	C
	112	BRAGFLO	A two-dimensional grid (one-degree dip) on the scale of the waste disposal region is used for DBR calculations.	Blowouts (H23)	R
	113	BRAGFLO CCDFGF	Calculation of DBR from several different locations provides reference results for the variation in release associated with the intrusion location and the degree of panel closures separating it from the location of a previous intrusion.	Blowouts (H23)	R
CRA-2004: 6.4.7.2 Long-Term Releases Following Drilling CRA-2019: MASS-14.3 Long-Term Properties of the Abandoned Intrusion Borehole	114	BRAGFLO CCDFGF	Plugging and abandonment of future boreholes are assumed to be consistent with current practices in the Delaware Basin.	Natural Borehole Fluid Flow (H31) Waste-Induced Borehole Flow (H32)	Reg.

Chapter or Section	Assumption Number	Code	Modeling Assumption	Related FEP in Appendix SCR-2019	Assumption Considered[a]
CRA-2004: 6.4.7.2.1 Continuous Concrete Plug through the Salado and Castile (Plug type VI in U.S. DOE 2018)	115	CCDFGF	A continuous concrete plug is assumed to exist throughout the Salado and Castile. Long-term releases through a continuous plug are analogous to releases through a sealed shaft.	Natural Borehole Fluid Flow (H31) Waste-Induced Borehole Flow (H32)	Reg.-R
CRA-2004: 6.4.7.2.2 The Two-Plug Configuration (Plug types I, III, and V in U.S. DOE 2018)	116	BRAGFLO	A lower plug is located between the Castile brine reservoir and underlying formations (as represented by a no flow boundary condition). A second plug is located immediately above the Salado. The brine reservoir and WP region are in direct communication though an open cased hole.	Natural Borehole Fluid Flow (H31) Waste-Induced Borehole Flow (H32)	Reg.-R
	117	BRAGFLO	The casing and upper concrete plug are assumed to fail after 200 years, and the borehole is assumed to be filled with silty-sand-like material. At 1,200 years after abandonment, the permeability of the borehole below the WP region is decreased by one order of magnitude as a result of salt creep.	Natural Borehole Fluid Flow (H31) Waste-Induced Borehole Flow (H32)	R
CRA-2004: 6.4.7.2.3 The Three-Plug Configuration (Plug types II and IV in U.S. DOE 2018)	118	CCDFGF	In addition to the two-plug configuration, a third plug is placed within the Castile above the brine reservoir. Te third plug is assumed not to fail over the regulatory time period.	Natural Borehole Fluid Flow (H31) Waste-Induced Borehole Flow (H32)	Reg.-R
CRA-2004: 6.4.8 Castile Brine Reservoir CRA-2019: MASS-16.0 Castile Brine Reservoir	119	BRAGFLO	Brine occurrences in the Castile are bounded systems. Brine reservoirs under the waste panels are assumed to have limited extent and interconnectivity, with effective radii on the order of several hundred meters (m).	Brine Reservoirs (N2)	R

Chapter or Section	Assumption Number	Code	Modeling Assumption	Related FEP in Appendix SCR-2019	Assumption Considered[a]
CRA-2004: 6.4.9 Climate Change CRA-2019: MASS-15.0 Climate Change	120	SECOTP2D	Climate-related factors are treated through recharge. A parameter called the Climate Index is used to scale the Culebra flux field.	Climate Change (N61) Temperature (N60) Precipitation (e.g., Rainfall) (N59)	R
CRA-2004: 6.4.10 Initial and Boundary Conditions for Disposal System Modeling CRA-2004: 6.4.10.1 Disposal System Flow and Transport Modeling (BRAGFLO and NUTS)	121	BRAGFLO	There are no gradients beyond the gravity-induced one-degree dip (south) for flow in the far-field of the Salado, and pressures are above hydrostatic but below lithostatic. Excavation and waste emplacement result in partial drainage of the DRZ.	Saturated Groundwater Flow (N23) Brine Inflow (W40)	R
	122	BRAGFLO	An initial water-table surface is set in the Dewey Lake at an elevation of 980 m (3,215 foot [ft]) above mean sea level. The initial pressures in the Salado are extrapolated from a sampled pressure in MB 139 at the shaft and are in hydrostatic equilibrium. The excavated region is assigned an initial pressure greater than one atmosphere (1.28039E5 Pa) to account for the incremental pressure generated by faster initial microbial gas generation rates observed during laboratory experiments. The liquid saturation of the waste-disposal region is consistent with the liquid saturation of emplaced waste. Other excavated regions are assigned zero liquid saturation, except the shaft, which is fully saturated.	Saturated Groundwater Flow (N23)	R
	123	NUTS	Molecular transport boundary conditions are no diffusion or dispersion in the normal direction across far-field boundaries. Initial An concentrations are zero everywhere, except in the waste.	Radionuclide Decay and Ingrowth (W12) Solute Transport (W77)	R

Chapter or Section	Assumption Number	Code	Modeling Assumption	Related FEP in Appendix SCR-2019	Assumption Considered[a]
CRA-2004: 6.4.10.2 Culebra Flow and Transport Modeling (MODFLOW-2000, SECOTP2D)	124	MODFLOW-2000	Constant head and no-flow boundary conditions are set on the far-field boundaries of the flow model.	Saturated Groundwater Flow (N23)	R
	125	MODFLOW-2000	Initial An concentrations in the Culebra are zero.	Solute Transport (W77)	R
CRA-2004: 6.4.10.3 Initial and Boundary Conditions for Other Computational Models	126	NUTS PANEL BRAGFLO (DBR) CUTTINGS_S	Initial and boundary conditions are interpolated from previously executed BRAGFLO calculations.	None	R
CRA-2004: 6.4.12 Sequences of Future Events CRA-2019: MASS-18.0 Evaluation of Waste Structural Impacts, Emplacement, and Homogeneity	127	CCDFGF	Each 10,000-year future (random sequence of future events) is generated by randomly and repeatedly sampling (1) the time between drilling events, (2) the location of drilling events, (3) the activity level of the waste penetrated by each drilling intrusion, (4) the plug configuration of the borehole, (5) the penetration of a Castile brine reservoir, and (6) the occurrence of mining in the disposal system.	Oil and Gas Exploration (H1) Potash Exploration (H2) Oil and Gas Exploitation (H4) Other Resources (H8) Enhanced Oil and Gas Recovery (H9) Natural Borehole Fluid Flow (N31) Waste-Induced Borehole Flow (H32)	Reg.-R
CRA-2004: 6.4.12.1 Active and Passive Institutional Controls in Performance Assessment	128	CCDFGF	Active institutional controls are effective for 100 years and completely eliminate the possibility of disruptive human activities (e.g., drilling and mining). No credit is taken for passive institutional controls.	None	Reg.-R

Chapter or Section	Assumption Number	Code	Modeling Assumption	Related FEP in Appendix SCR-2019	Assumption Considered[a]
CRA-2004: 6.4.12.2 umber and Time of Drilling Intrusions	129	CCDFGF	Drilling may occur after 100 years according to a Poisson process.	Loss of Records (H57) Oil and Gas Exploration (H1) Potash Exploration (H2) Oil and Gas Exploitation (H4) Other Resources (H8)	Reg.-R
CRA-2004: 6.4.12.3 Location of Intrusion Boreholes CRA-2019: MASS-14.2 Direct Brine Releases during Drilling	130	CCDFGF	The waste disposal region is represented by 10 regions (corresponding to 10 panels), each with a probability of being intersected proportional to its assumed footprint. A single borehole can penetrate only one region. The region/panel neighbor relationship for two panels is defined as “adjacent” for panels with one or fewer intact panel closures between them and “non-adjacent” for panels with more than one intact panel closure between them (Zeitler et al. 2017).	Disposal Geometry (W1)	R
CRA-2004: 6.4.12.4 Activity of the Intersected Waste Appendix TRU WASTE-2004 CRA-2019: MASS-14.1.4 Calculation of Cuttings, Cavings, and Spallings Releases	131	CCDFGF	Five hundred ten (510) waste streams are identified as contact-handled transuranic (CH-TRU) and 97 waste streams are identified as remote-handled transuranic (RH-TRU) (Kicker 2019). For each of the CH and RH cases, cuttings and cavings activities are derived from individual waste streams, with a probability of intersection based on the relative waste stream volume. Spallings concentrations are equal to the average CH-TRU concentration.	Heterogeneity of Waste Forms (W3)	R

Chapter or Section	Assumption Number	Code	Modeling Assumption	Related FEP in Appendix SCR-2019	Assumption Considered[a]
CRA-2004: 6.4.12.5 Diameter of the Intrusion Borehole	132	CUTTINGS_S	The diameter of the intrusion borehole is constant at 12.25 inches (in.) (31.12 centimeters [cm]).	None	Reg.-R
CRA-2004: 6.4.12.6 Probability of Intersecting a Brine Reservoir	133	CCDFGF	The probability that a deep borehole intersects the single brine reservoir below the waste panels is sampled from a defined distribution and has been updated for the CRA-2019 PA (Zeitler 2019c, Kim and Feng 2019).	Brine Reservoirs (N2)	R
CRA-2004: 6.4.12.7 Plug Configuration in the Abandoned Intrusion Borehole	134	CCDFGF	The two-plug configuration has a probability of 0.331. The three-plug configuration has a probability of 0.266. The continuous concrete plug has a probability of 0.403 (Kim and Feng 2019).	None	Reg.-R
CRA-2004: 6.4.12.8 Probability of Mining Occurring in the Land Withdrawal Area	135	CCDFGF	Mining in the disposal system occurs a maximum of once in 10,000 years (a 10^{-4} probability per year).	None	Reg.-R
CRA-2004: 6.4.13 Construction of a Single Complementary Cumulative Distribution Function (CCDF)	136	CCDFGF	Deterministic calculations from BRAGFLO, NUTS, MODFLOW-2000, SECOTP2D, CUTTINGS_S, DRSPALL, and PANEL are used to generate reference conditions that are used to estimate the consequences associated with random sequences of future events. These are, in turn, used to develop CCDFs.	None	R
	137	CCDFGF	Ten thousand random sequences of future events are generated for each CCDF plotted.	None	R
CRA-2004: 6.4.13.1 Constructing Consequences of the Undisturbed Performance Scenario	138	CCDFGF	A BRAGFLO and NUTS calculation with undisturbed conditions is sufficient for estimating the consequences of the undisturbed performance scenario.	None	R

Chapter or Section	Assumption Number	Code	Modeling Assumption	Related FEP in Appendix SCR-2019	Assumption Considered[a]
CRA-2004: 6.4.13.2 Scaling Methodology for Disturbed Performance Scenarios	139	CCDFGF	Consequences for random sequences of future events are constructed by scaling the consequences associated with deterministic calculations (reference conditions) to other times, generally by interpolation, but sometimes by assuming either similarity or no consequence.	None	R
CRA-2004: 6.4.13.3 Estimating Long-Term Releases from the E1 Scenario	140	CCDFGF NUTS	Reference conditions are calculated or estimated for intrusions at 100, 350, 1,000, 3,000, 5,000, 7,000, and 9,000 years. For multiple E1 intrusions into the same panel, the additional source term to the Culebra for the second and subsequent intrusions is assumed to be negligible.	Waste-Induced Borehole Flow (H32)	R
CRA-2004: 6.4.13.4 Estimating Long-Term Releases from the E2 Scenario	141	CCDFGF NUTS SECOTP2D	The methodology is similar to the methodology for the E1 scenario. For multiple E2 intrusions into the same panel, the additional source term to the Culebra for the second and subsequent intrusions is assumed to be negligible.	Waste-Induced Borehole Flow (H32) Waste Inventory (W2)	R
CRA-2004: 6.4.13.5 Estimating Long-Term Releases from the E1E2 Scenario	142	CCDFGF PANEL	The concentration of An in liquid moving up the borehole assumes homogeneous mixing within the panel.	Waste-Induced Borehole Flow (H32)	C
	143	PANEL	Any An that enter the borehole for long-term flow calculations reach the Culebra.	Waste-Induced Borehole Flow (H32)	C
	144	CCDFGF PANEL	Reference conditions are calculated or estimated for intrusion at 100, 350, 1,000, 2,000, 4,000, 6,000 and 9,000 years.	Oil and Gas Exploration (H1)	—

Chapter or Section	Assumption Number	Code	Modeling Assumption	Related FEP in Appendix SCR-2019	Assumption Considered[a]
CRA-2004: 6.4.13.6 Multiple Scenario Occurrences	145	CCDFGF PANEL	The panels are assumed not to be interconnected for long-term brine flow, although due to the open panel closure area modeled between the SROR and WP, some communication among panels effectively exists (Zeitler et al. 2017).	Saturated Groundwater Flow (N23) Unsaturated Groundwater Flow (N24)	R
CRA-2004: 6.4.13.7 Estimating Releases During Drilling for All Scenarios	146	CCDFGF PANEL NUTS	Repository conditions will be dominated by Castile brine if any borehole connects to a brine reservoir.	Brine Reservoirs (N2) Natural Borehole Fluid Flow (H31)	R
	147	CUTTINGS_S PANEL CCDFGF	Depletion of An in parts of the repository penetrated by boreholes is not accounted for in calculating the releases from single and subsequent intrusions at such locations.	Waste-Induced Borehole Flow (H32) Waste Inventory (W2)	C
CRA-2004: 6.4.13.8 Estimating Releases in the Culebra and the Impact of the Mining Scenario	148	CCDFGF	Releases from intrusions at random times in the future are scaled from releases calculated at 100 years with a unit source of radionuclides in the Culebra.	None	R
	149	CCDFGF	An in transit in the Culebra when mining occurs are transported in the flow field used for the undisturbed case. An introduced subsequent to mining are transported in the flow field used for the disturbed case (i.e., the mined case).	None	R

a R = Reasonable
C = Conservative
Reg. = Based on regulatory guidance

MASS-2.1 Darcy's Law Applied to Fluid Flow Calculated by BRAGFLO, MODFLOW-2000, and DRSPALL

The application of Darcy's Law to the fluid flow assumptions in WIPP PA has not changed since the CRA-2014 PA. A mathematical relationship expressing fluid flux as a function of hydraulic head gradients in a porous medium, commonly known as Darcy's Law, is applied to geologic

media for all fluid-flow calculations. For details about the specific formulation of Darcy's Law used in these calculations, refer to Appendix PA-2019, Section PA-4.2 for the disposal system and Section PA-4.8 for the Culebra. Darcy's Law is not applied for flow up a borehole being drilled (see Section MASS-14.2; the CRA-2004, Chapter 6.0, Section 6.4.7.1.1; and Appendix PA-2019, Section PA-4.7 for more discussion of this topic).

Darcy's Law generally applies to flow models for which certain conditions are satisfied: (1) the flow occurs in a porous medium with interconnected porosity, (2) flow velocities are low enough that viscous forces dominate inertial forces, and (3) a threshold hydraulic gradient is exceeded. In the CCA, Appendix MASS, these conditions were shown to be valid for the WIPP PA.

Darcy's Law assumes laminar flow; that is, there is no motion of the fluid at the fluid/solid interface and velocity increases with distance from the fluid/solid interface. For liquids, it is reasonable to assume laminar flow under most conditions, including those found in and surrounding the WIPP repository. For gases at low pressure, however, gas molecules near the solid interface may not have intimate contact with the solid and may have finite, non-zero velocity. This effect, which results in additional flux of gas above that predicted by application of Darcy's Law, is known as the slip phenomenon, or Klinkenberg effect (Bear 1972, p. 128). A correction to Darcy's Law for the Klinkenberg effect is incorporated into the BRAGFLO model (see Appendix PA-2019, Section PA-4.2).

Darcy flow for one and two phases implies that values for principal fluid and rock parameters must be specified. Fluid properties in the Darcy flow model used for the WIPP PA are density, viscosity, and compressibility, while rock properties are porosity, permeability, and compressibility (pore or bulk). In BRAGFLO, other parameters are required to describe the interactions or interference between the gas and brine phases present in the model because those phases can occupy the same pore space. In the WIPP application of Darcy flow models, compressibility of both the liquid and rock are related to porosity through a dependence on pressure. Fluid density, viscosity, and compressibility are functions of fluid composition, pressure, and temperature. It is assumed in BRAGFLO that fluid (both brine and gas) density and compressibility are pressure dependent, but fluid (both brine and gas) viscosity is constant. Fluid composition for the purposes of modeling flow and transport is assumed to be constant.

MASS-2.2 Hydrogen Gas as Surrogate for Waste-Generated Gas Physical Properties in BRAGFLO and DRSPALL

The use of hydrogen gas as a surrogate for waste-generated gas in WIPP PA has not changed since the CRA-2014 PA. Hydrogen gas is produced as a result of the corrosion of steel in the repository by water or brine and due to the radiolysis of water or brine in the repository. As in the CCA, the gas phase in the BRAGFLO model is assigned the properties of hydrogen because hydrogen will, under most conditions reasonable for the WIPP, be the dominant component of the gas phase. The model for spallings as implemented in the code DRSPALL also assigns the physical properties of hydrogen to the gas phase. As discussed in the following text, the effect of assuming flow of pure H_2 instead of a mixture of gases (including H_2, CO_2, and H_2S), can be shown to be minor relative to the permeability variations in the surrounding formations.

Other gases may be produced by processes occurring in the repository. If microbial degradation occurs, a significant amount of CO_2 and H_2S will be generated by microbial degradation of cellulosics and, possibly, plastics and rubbers in the waste. The CO_2 produced, however, will react with the magnesium-oxide (MgO) engineered barrier and cementitious materials to form brucite ($Mg(OH)_2$), hydromagnesite ($Mg_5(CO_3)_4(OH)_2{\cdot}4H_2O$), and calcite ($CaCO_3$), thus resulting in very low CO_2 fugacity in the repository. The H_2S generated by microbial degradation is assumed to persist and is treated as H_2 in PA calculations. Although other gases exist in the disposal system, BRAGFLO calculations assume these gases are insignificant and they are not included in the model.

With the average stoichiometry gas generation model, the total number of moles of gas generated will be the same whether the gas is considered to be pure H_2 or a mixture of several gases, because the generation of other gases is accounted for by specifying the stoichiometric factor for microbial degradation of cellulose (see Appendix GEOCHEM-2019, Section GEOCHEM-2.4). Therefore, considering only the moles of gas generated, the pressure buildup in the repository will be approximately the same because the expected gases behave similarly to an ideal gas, even up to lithostatic pressures.

The effect of assuming pure H_2 instead of a mixture of gases (including H_2, CO_2, and H_2S) on flow behavior, and its resulting impact on the WIPP repository pressure, is described in detail in Appendix MASS-2014, Section 3.2 and is summarized below. Viscosity has an inverse relationship to flow rate and a direct relationship to the square of the repository pressure. Hence, viscosity differences that would result if gas properties other than those of hydrogen were incorporated would result in a decrease in flow rate and potentially higher pressures. Like viscosity, the gas compressibility (actual volume/ideal volume) is inversely related to flow rate and directly related to the square of the repository pressure. Therefore, the impact of variation in gas compressibility caused by composition would be minor and it is not considered.

The permeability of each component of the formation plays a significant role in determining both flow rate and pressure. Because MB permeabilities and Salado impure halite permeabilities vary over three to four orders of magnitude (Kim and Feng 2019), the permeabilities of these flow pathways will have a greater influence on pressure and flow rate determinations than either uncertainty in viscosity or gas compressibility effects.

Note also that the BRAGFLO code includes a pressure-induced fracture model that will limit pressure increases in the repository (Schreiber 1997). For example, at high repository pressures, the factor of 1.5 pressure increase calculated here using the simplified Darcy's Law model is unlikely to be seen in the BRAGFLO results, since fracturing will lead to increased permeability, effectively limiting pressure increases.

MASS-2.3 Salado Brine as Surrogate for Liquid-Phase Physical Properties in BRAGFLO

The use of Salado brine as a surrogate for liquid phases in WIPP PA has not changed since the CRA-2014 PA. BRAGFLO uses Salado Formation brine properties as the physical properties for all liquids. However, liquid in the modeled region may consist of (1) brine originally in the Salado, (2) liquid introduced in the excavation during construction, maintenance, and ventilation

during the operational phase, (3) a very small amount of liquid introduced as a component of the waste, (4) liquid from overlying units, and (5) liquid from the Castile brine reservoir. However, for BRAGFLO modeling, it is assumed that the properties of all of these liquids are similar enough to Salado brine properties that the effect of any variation in properties resulting from liquids mixing is negligible. The variations in chemical properties of brine are accounted for as discussed in Appendix SOTERM-2019, Section SOTERM-2.0, and Appendix GEOCHEM-2019, Section GEOCHEM-3.1.

MASS-3.0 Model Geometries

This section presents supplementary information on the disposal system geometry and includes the representation of intact and open panel closure areas in that discussion. The principal process considered in defining the repository geometry is fluid flow. The model geometries implemented in WIPP PA have changed since the CRA-2014 PA, as described below.

MASS-3.1 Disposal System Geometry as Modeled in BRAGFLO

The geometry used to represent long-term fluid flow processes in the Salado, flow between a borehole and overlying units, and flow within the repository (where processes coupled to fluid flow such as creep closure and gas generation occur), is a vertical cross section through the repository on a north-south axis (see also Appendix PA-2019, Section PA-4.2.1). The dimension of this geometry in the direction perpendicular to the plane of the cross section varies so that spatial effects of repository processes can be represented. Use of a two-dimensional geometry to represent the three-dimensional Salado flow is based on the assumption that brine and gas flow will converge upon and diverge from the repository horizon. Above and below the repository, it is assumed that any flow between the borehole or shaft (see CRA-2004, Chapter 6.0, Section 6.4.3) and surrounding materials will converge or diverge. Grid flaring is used in the BRAGFLO disposal system geometry, and flows are represented as divergent and convergent from the flaring center (see Appendix MASS-2014, Section MASS-4.1.1.4). The impact of this implementation in a two-dimensional grid has been compared to a model that does not make the assumption of convergent and divergent flow (see Appendix PA-2004, Attachment MASS, Attachment 4-1 for additional information). The BRAGFLO representation of the Salado also includes the slight and variable dip of beds in the vicinity of the repository. Below the repository, the possible presence of a brine reservoir is considered to be important, so a hydrostratigraphic layer representing the Castile and a possible brine reservoir in it is included (see the CCA, Appendix MASS, Section MASS-4.2 for the disposal system geometry historical context prior to the CCA).

For modeling brine flow from the intruded panel to the borehole during drilling, the geometry represented in BRAGFLO is a two-dimensional, horizontal representation of the repository waste area as described in Section MASS-14.2.

Changes have been made to the disposal system geometry representation in BRAGFLO since that implemented in the CCA. The evolution of these changes from the CCA through the CRA-2014 PA is discussed in Appendix MASS 2014. Changes to the disposal system geometry representation in BRAGFLO between the CRA-2014 PA and CRA-2019 PA are discussed below.

MASS-3.1.1 CRA-2014 to CRA-2019 Baseline Grid Changes

The BRAGFLO material map and numerical grid used in the CRA-2019 PA has been updated from that used for the CRA-2014 PA. There are four differences between the CRA-2014 PA grid and the CRA-2019 PA grid:

1. The x-dimension of the columns containing the northernmost panel closure area has been doubled to correct an error in the CRA-2014 PA grid (Zeitler 2019a);

2. The x- and z-dimensions of the column containing the shaft representation have been updated to incorporate a fifth shaft (Zeitler 2019b);

3. The z-dimensions of the columns containing the EXP area have been updated to incorporate the volume of the drifts associated with the fifth shaft (Zeitler 2019b); and

4. The southernmost panel closure area is now referred to as an "abandoned panel closure" area due to the decision to not emplace panel closures in Panels 3, 4, 5, and 6 (Zeitler et al. 2017). The DRZ and MB areas above and below the southernmost panel closure area are treated in a similar manner to those above and below the OPS and EXP areas.

Figure MASS-1 shows the BRAGFLO grid, including updated dimensions and names labeled for each area of the repository and its surroundings. Figure MASS-2 through Figure MASS-11 show material maps associated with the BRAGFLO grid for all BRAGFLO scenarios across all time periods (-5 to 10,000 y). Associations between the material maps and BRAGFLO scenarios (Table MASS-2) are summarized in Table MASS-3.

Table MASS-2. WIPP PA BRAGFLO Scenarios

Scenario	No. of Drilling Intrusions	Time of Intrusion (Years)	Castile Brine Pocket Encountered?
S1-BF	0 (Undisturbed)	NA	NA
S2-BF	1	350	Yes
S3-BF	1	1,000	Yes
S4-BF	1	350	No
S5-BF	1	1,000	No
S6-BF	2	1,000 and 2,000	Only at 2,000 y

Table MASS-3. Time Period Associations Between Material Map Figures and WIPP PA BRAGFLO Scenarios

Scenario	Material Map Figure Number and Associated Time Period (y)									
	Figure MASS-2	**Figure MASS-3**	**Figure MASS-4**	**Figure MASS-5**	**Figure MASS-6**	**Figure MASS-7**	**Figure MASS-8**	**Figure MASS-9**	**Figure MASS-10**	**Figure MASS-11**
S1-BF	-5 - 0	0 - 100	100 - 200	200 -10000	-	-	-	-	-	-
S2-BF	-5 - 0	0 - 100	100 - 200	200 - 350	-	-	350-550	-	550 - 1550	1550 - 10000
S3-BF	-5 - 0	0 - 100	100 - 200	200 - 1000	-	-	1000 - 1200	-	1200 - 2200	2200 - 10000
S4-BF	-5 - 0	0 - 100	100 - 200	200 - 350	350 - 550	550 - 10000	-	-	-	-
S5-BF	-5 - 0	0 - 100	100 - 200	200 - 1000	1000 - 1200	1200 - 10000	-	-	-	-
S6-BF	-5 - 0	0 - 100	100 - 200	200 - 1000	1000 - 1200	1200 - 2000	-	2000 - 2200	2200 - 3200	3200 - 10000

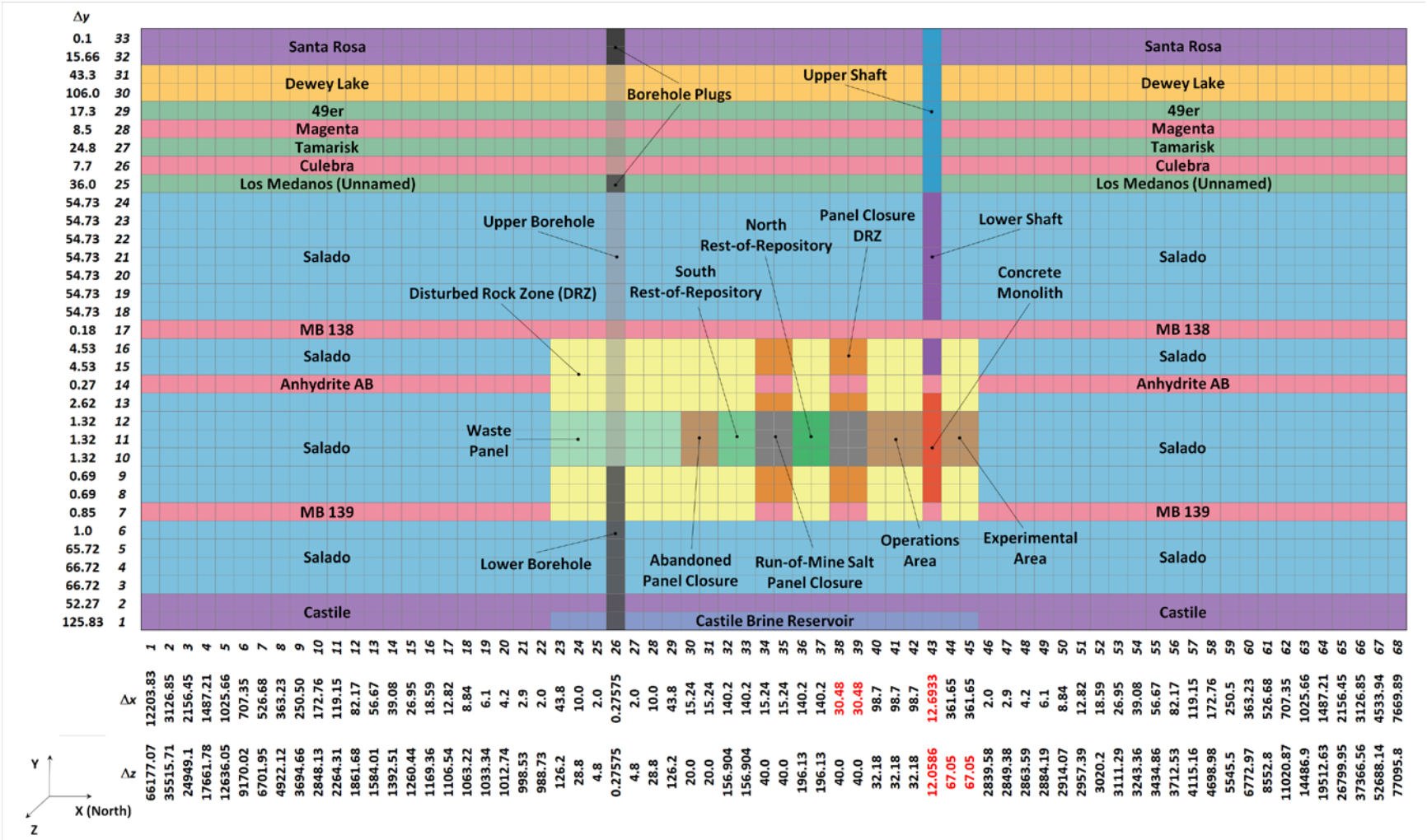

Figure MASS-1. Generic CRA-2019 PA BRAGFLO Grid with Modeled Area Descriptions (Δx, Δy, and Δz Dimensions in Meters)

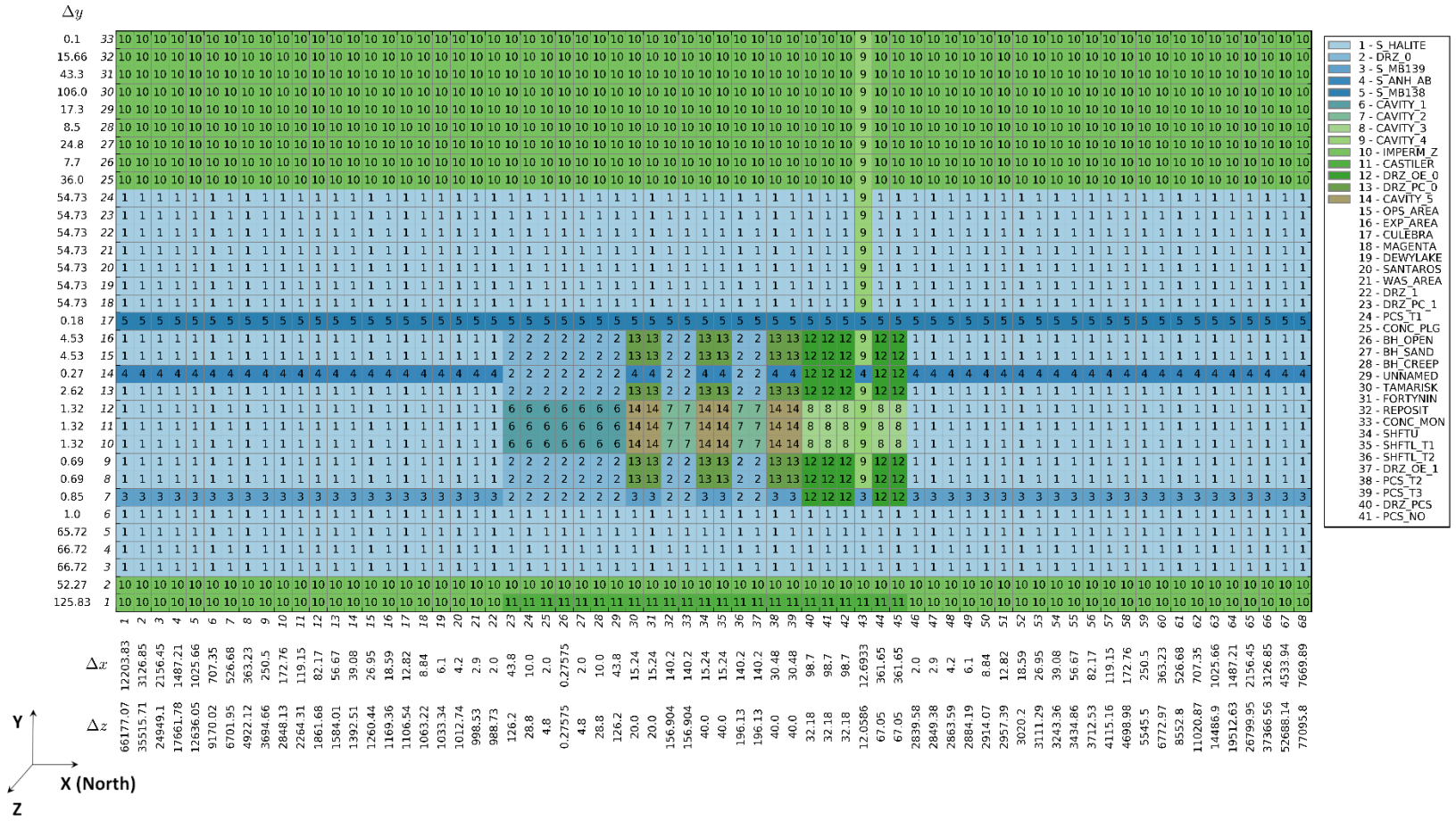

Figure MASS-2. CRA-2019 PA BRAGFLO Grid and Material Map; Years -5 to 0 [Scenarios S1-BF through S6-BF] (Δx, Δy, and Δz Dimensions in Meters)

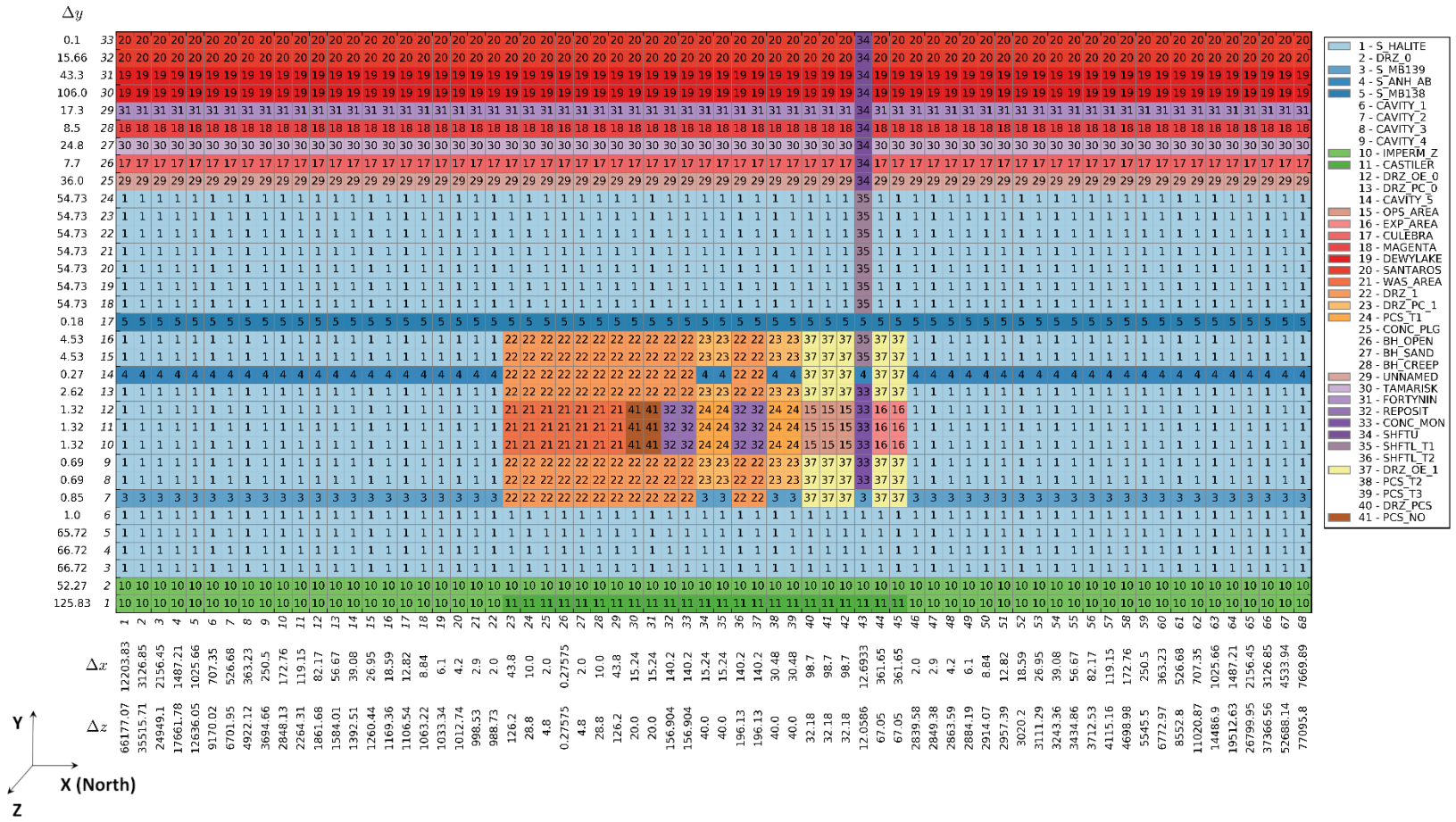

Figure MASS-3. CRA-2019 PA BRAGFLO Grid and Material Map; Years 0 to 100 [Scenarios S1-BF through S6-BF] (Δx, Δy, and Δz Dimensions in Meters)

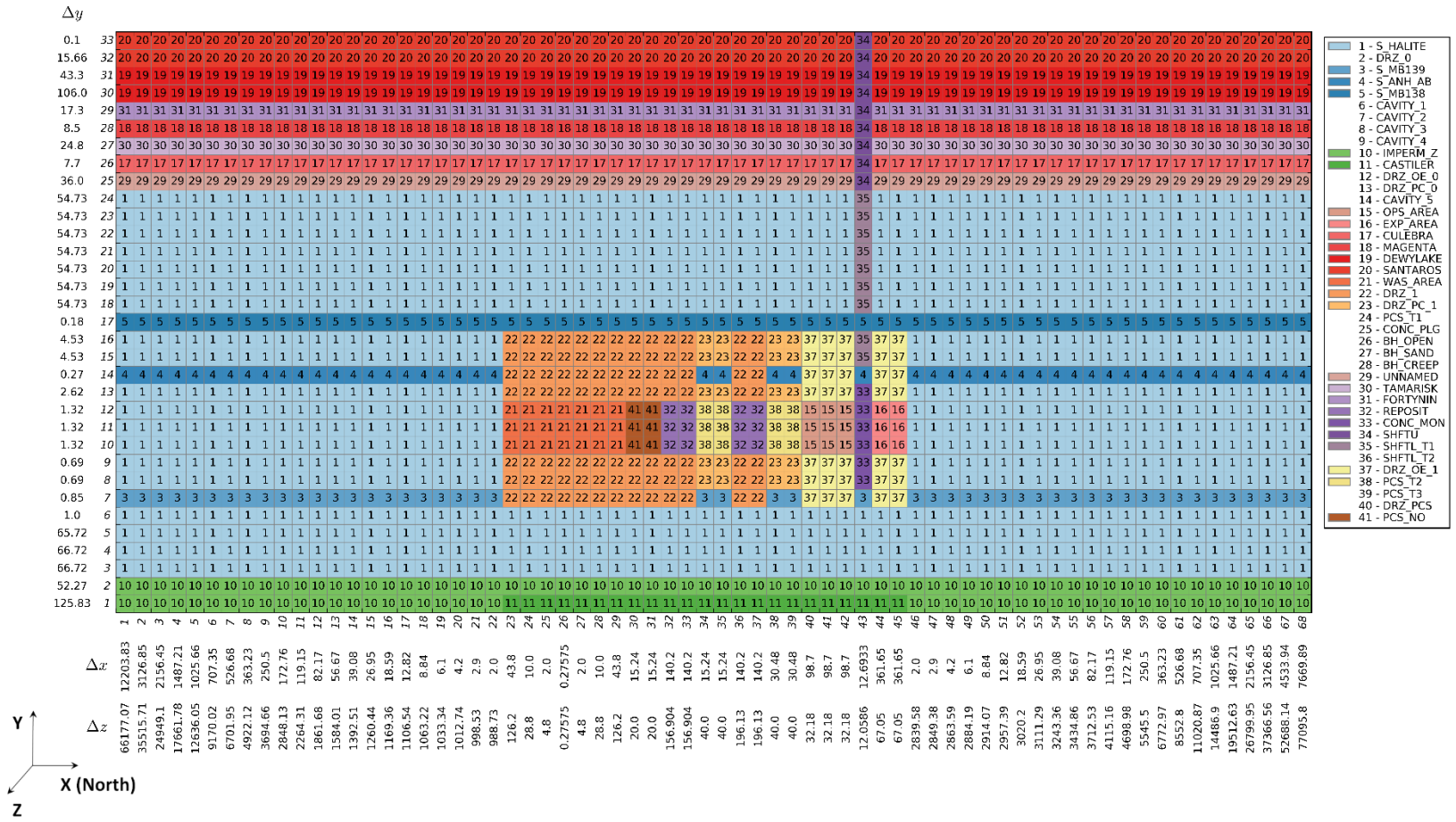

Figure MASS-4. CRA-2019 PA BRAGFLO Grid and Material Map; Years 100 to 200 [Scenarios S1-BF through S6-BF] (Δx, Δy, and Δz Dimensions in Meters)

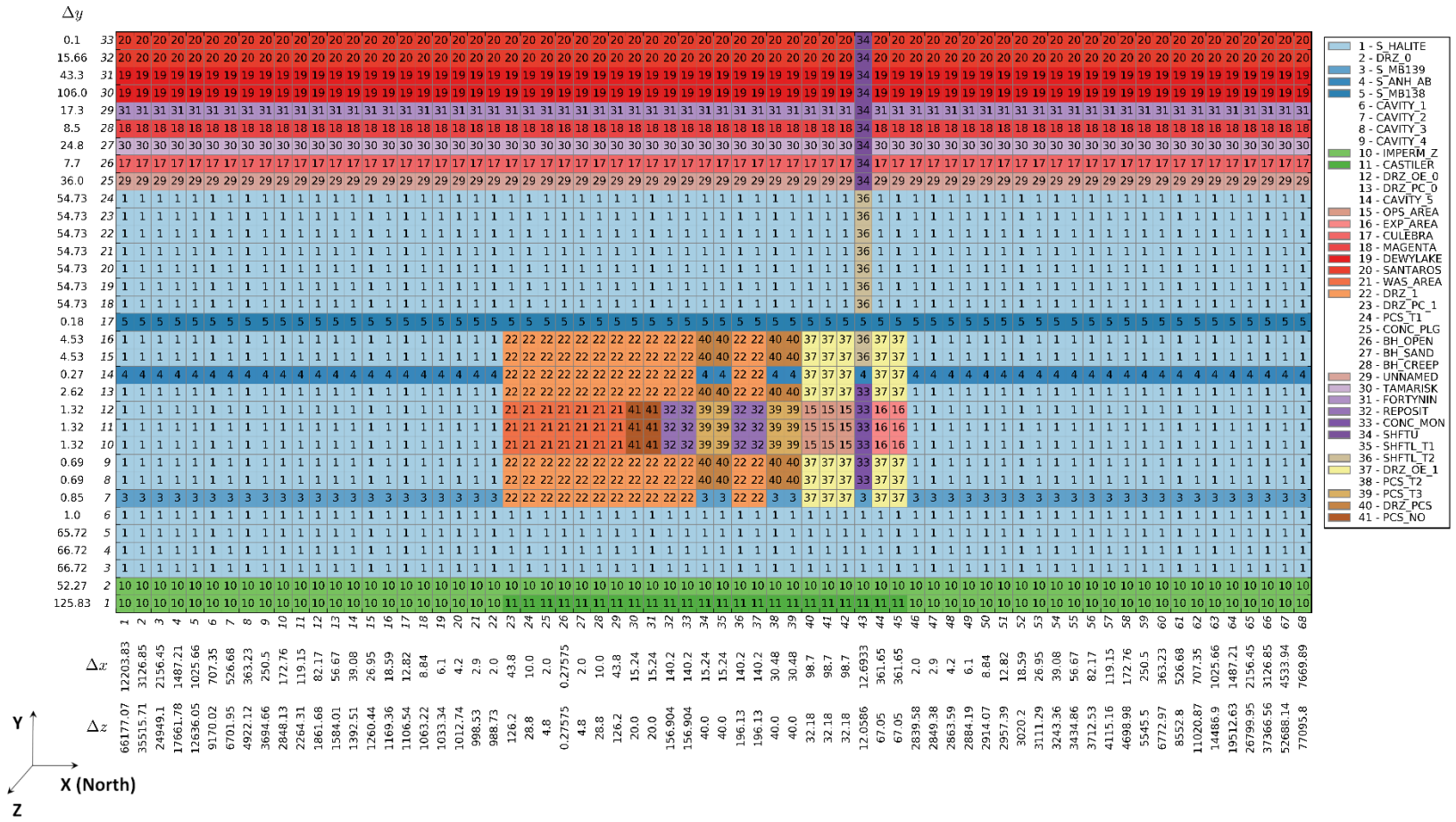

Figure MASS-5. CRA-2019 PA BRAGFLO Grid and Material Map; Years 200 to 10000 [Scenario S1-BF], Years 200 to Time of E1 or E2 Intrusion [Scenarios S2-BF through S6-BF] (Δx, Δy, and Δz Dimensions in Meters)

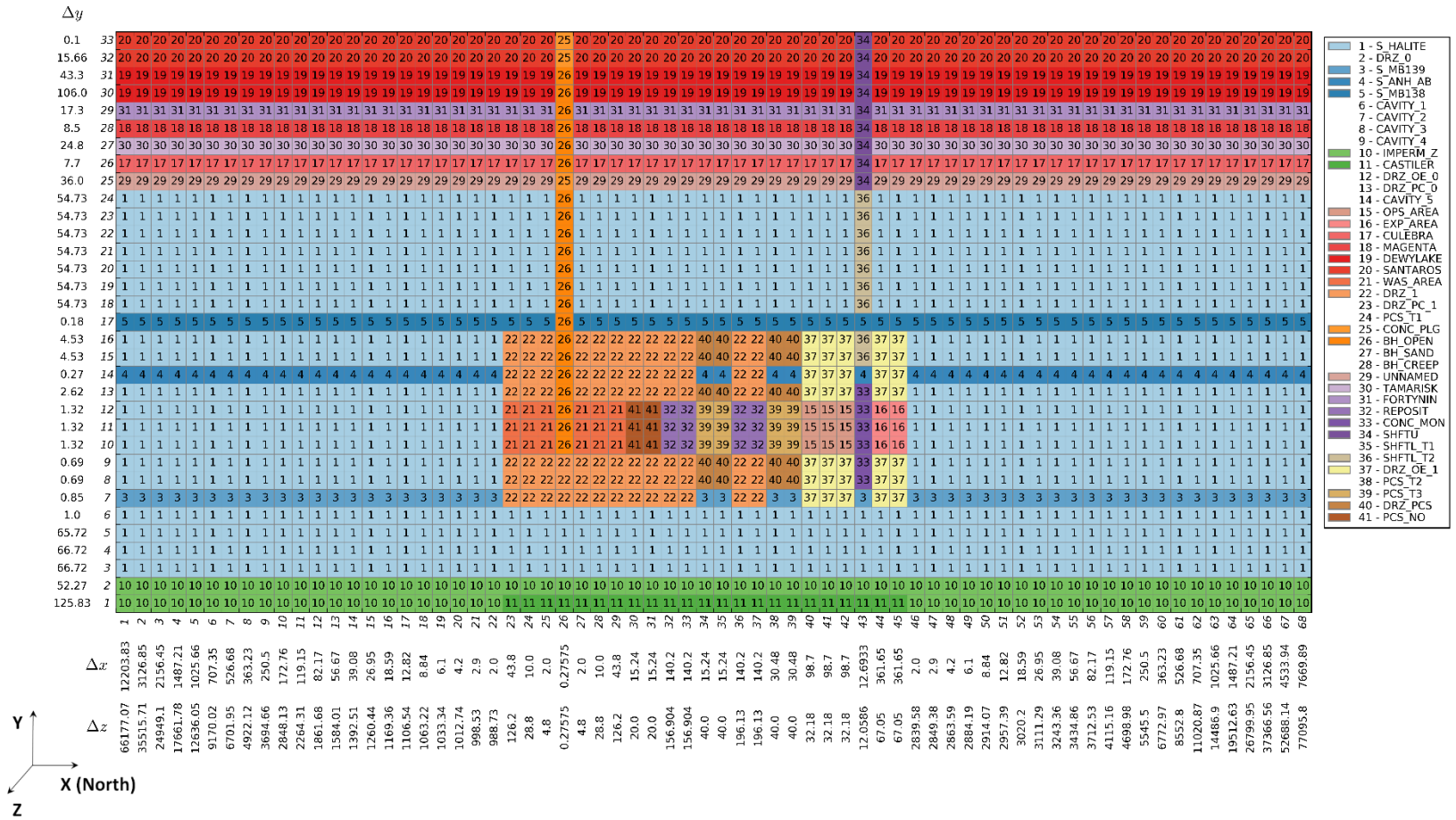

Figure MASS-6. CRA-2019 PA BRAGFLO Grid and Material Map; Time of E2 Intrusion to Time of E2 Intrusion Plus 200 Years [Scenarios S4-BF through S6-BF] (Δx, Δy, and Δz Dimensions in Meters)

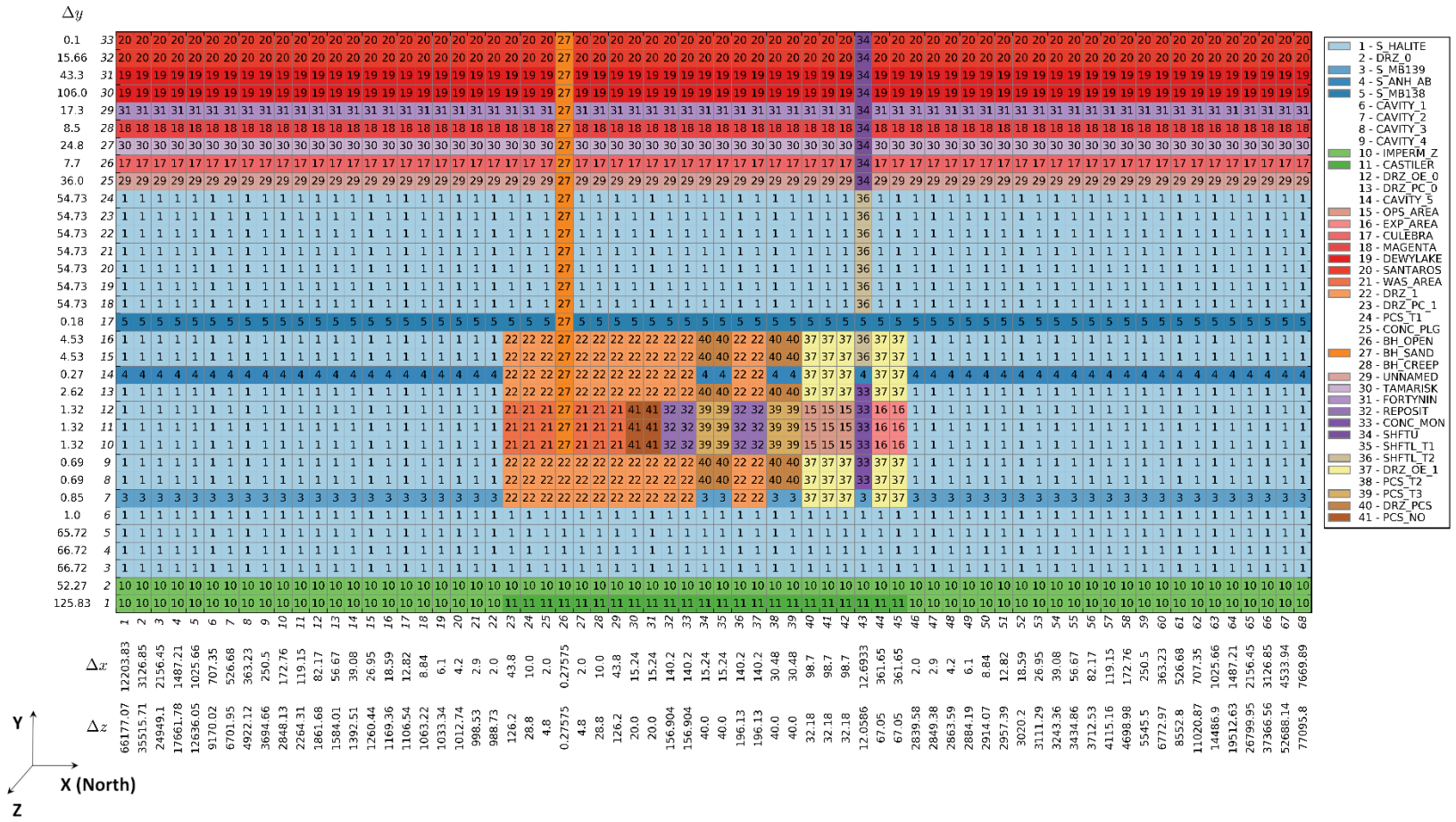

Figure MASS-7. CRA-2019 PA BRAGFLO Grid and Material Map; Time of E2 Intrusion Plus 200 Years to 10000 Years [Scenarios S4-BF and S5-BF], Time of E2 Intrusion Plus 200 Years to Time of E1 Intrusion [Scenario S6-BF] (Δx, Δy, and Δz Dimensions in Meters)

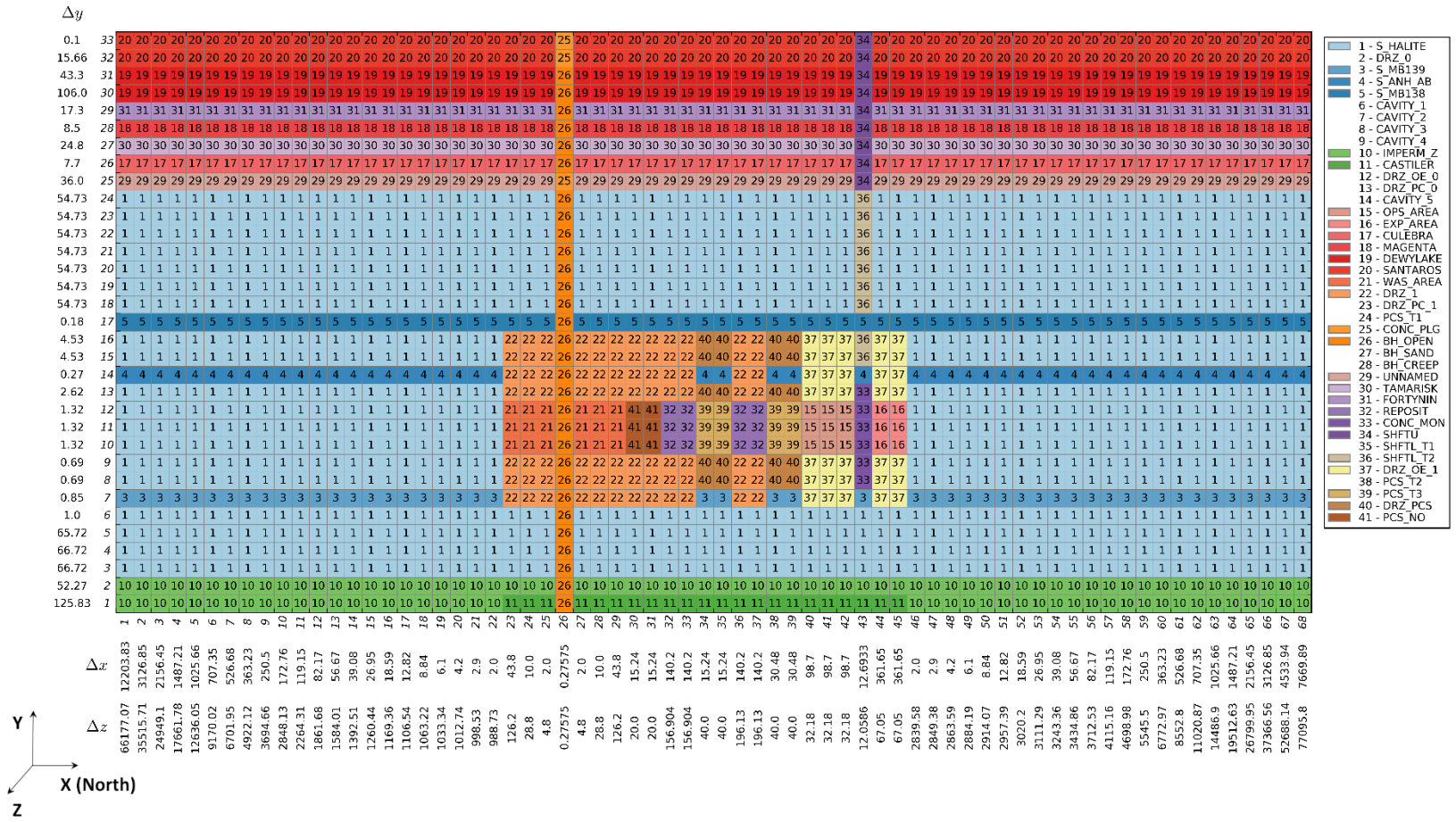

Figure MASS-8. CRA-2019 PA BRAGFLO Grid and Material Map; Time of E1 Intrusion to Time of E1 Intrusion Plus 200 Years [Scenarios S2-BF and S3-BF] (Δx, Δy, and Δz Dimensions in Meters)

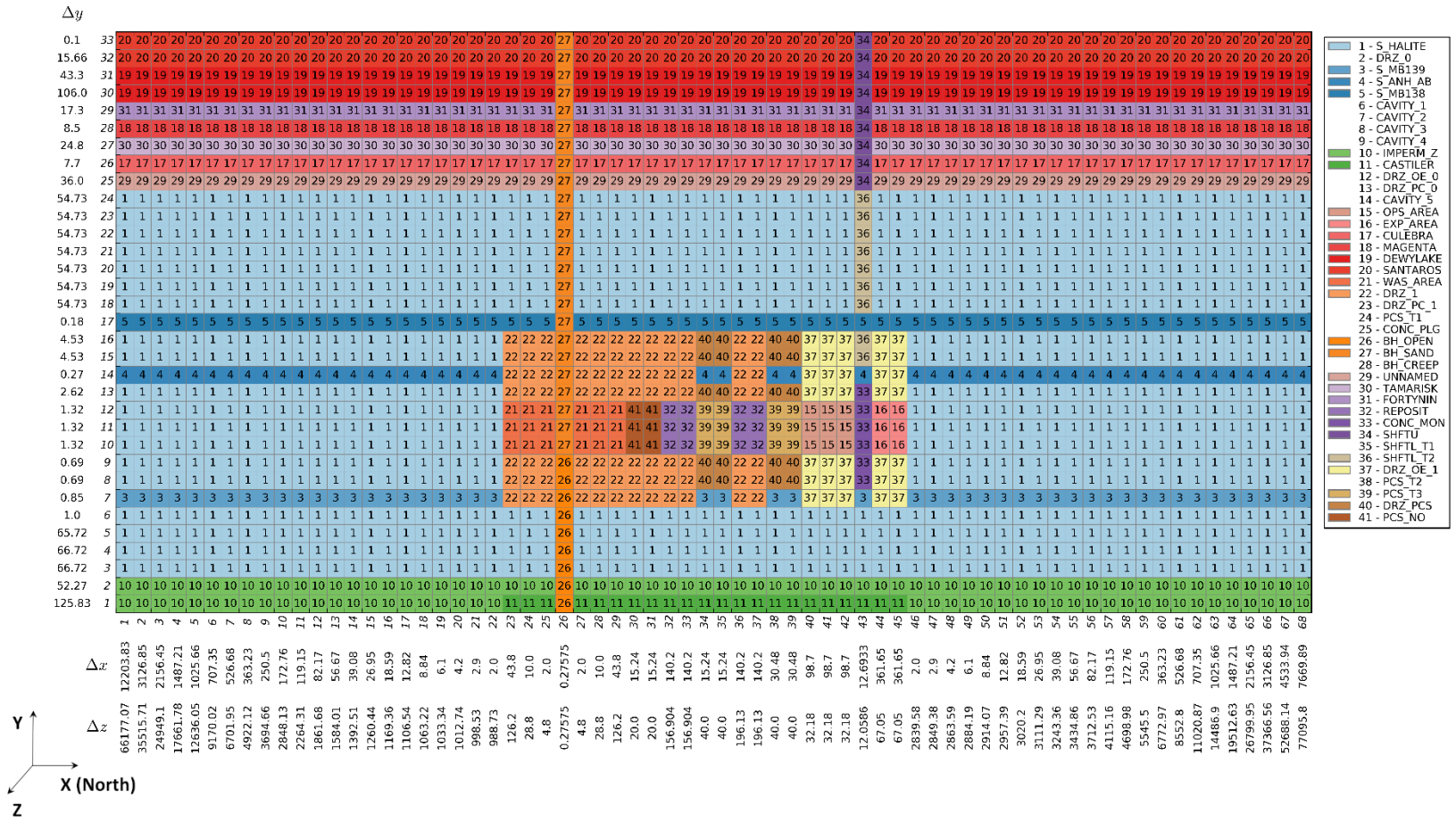

Figure MASS-9. CRA-2019 PA BRAGFLO Grid and Material Map; Time of E1 Intrusion to Time of E1 Intrusion Plus 200 Years [Scenario S6-BF] (Δx, Δy, and Δz Dimensions in Meters)

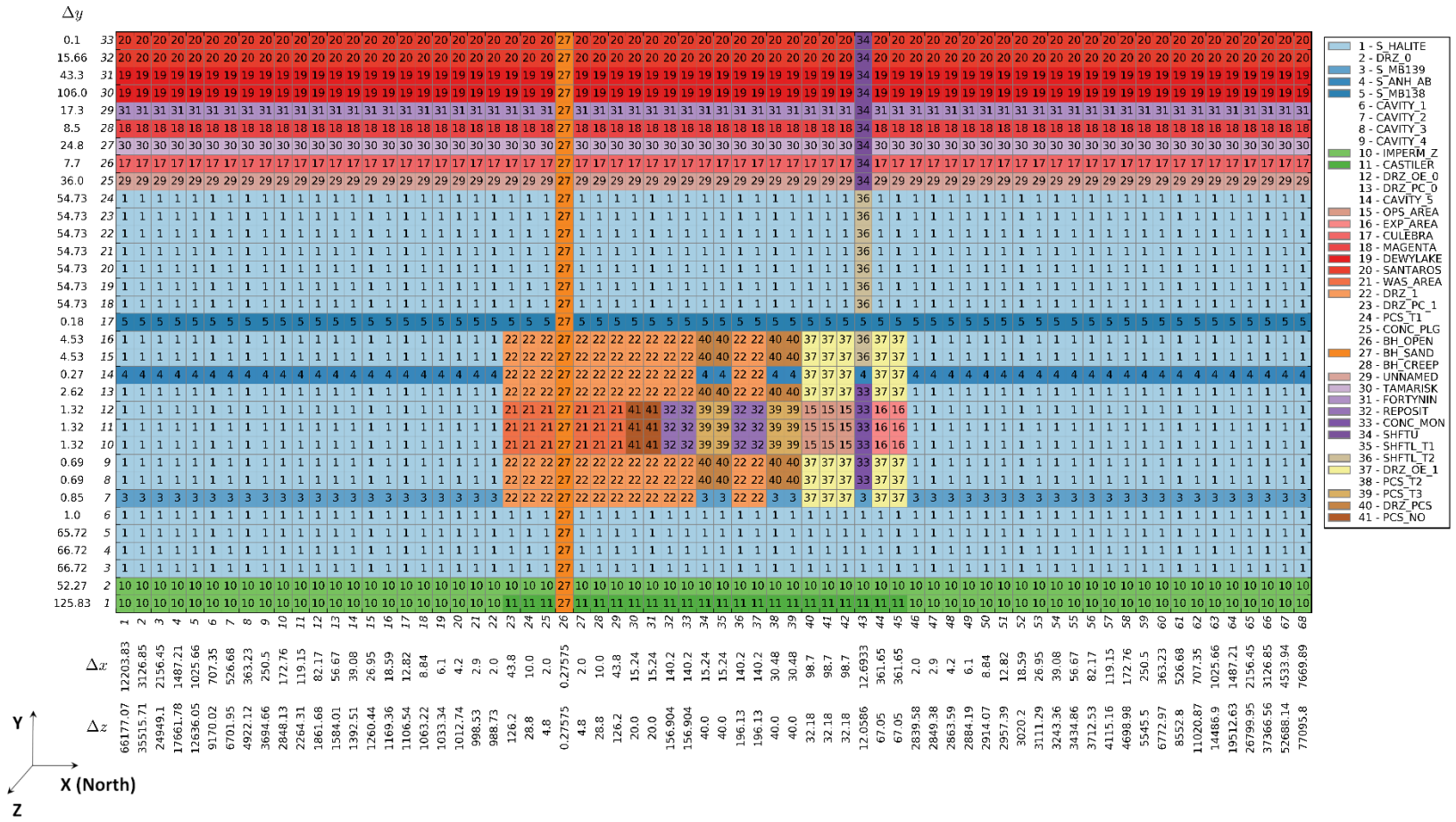

Figure MASS-10. CRA-2019 PA BRAGFLO Grid and Material Map; Time of E1 Intrusion Plus 200 Years to Time of E1 Intrusion Plus 1200 Years [Scenarios S2-BF, S3-BF, and S6-BF] (Δx, Δy, and Δz Dimensions in Meters)

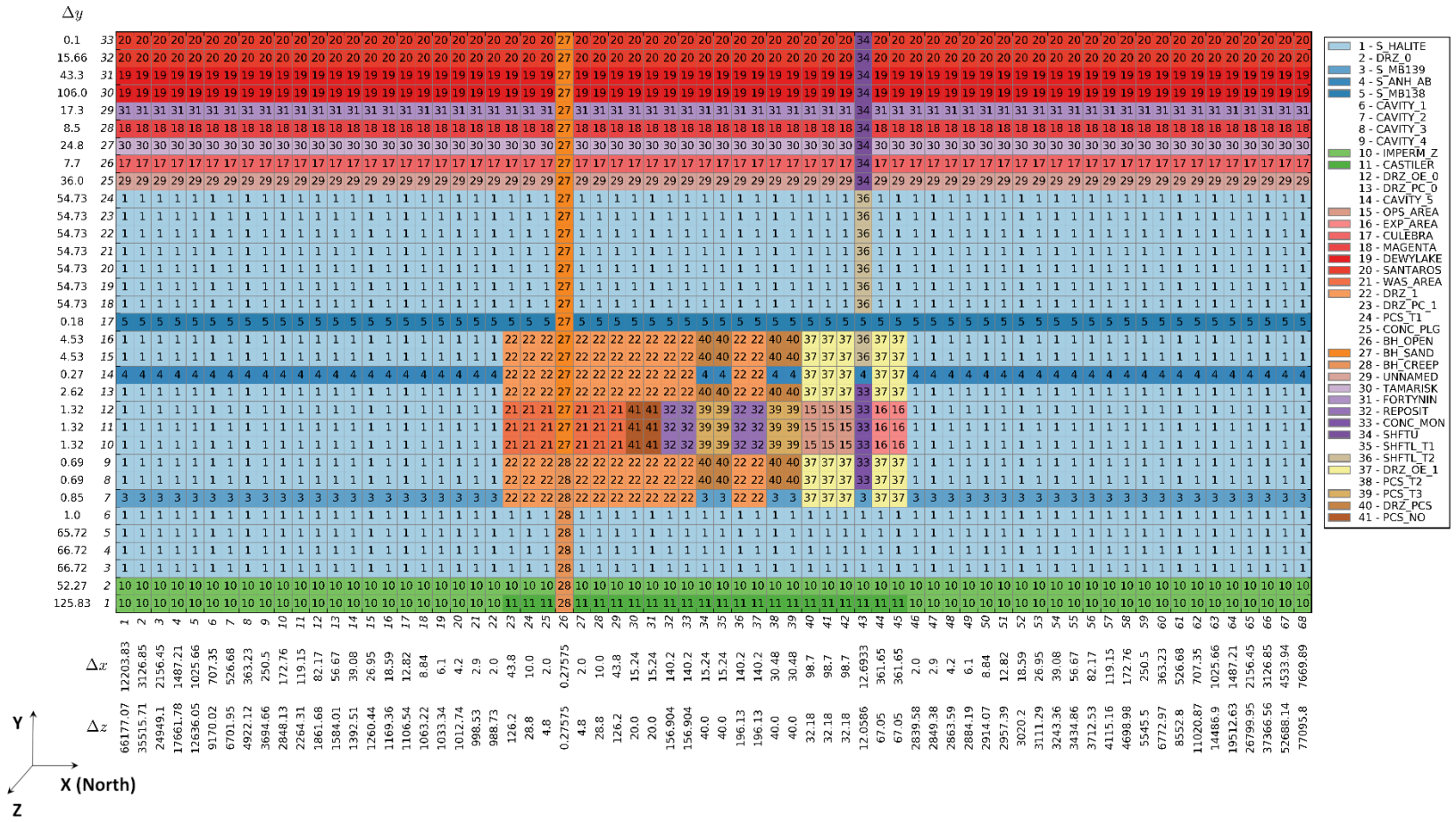

Figure MASS-11. CRA-2019 PA BRAGFLO Grid and Material Map; Time of E1 Intrusion Plus 1200 Years to 10000 Years [Scenarios S2-BF, S3-BF, and S6-BF] (Δx, Δy, and Δz Dimensions in Meters)

MASS-4.0 Creep Closure

The creep closure model used in the CRA-2019 PA is the same as that used in the CRA-2014 PA. The model used for creep closure of the repository is discussed in Appendix PORSURF-2014. Historical information on creep closure modeling is also contained in Appendix PORSURF-2014.

MASS-5.0 Repository Fluid Flow

Repository fluid flow assumptions have changed from those used in the CRA-2014 PA. Radiolytic gas generation, which consumes water, has been added to the gas generation model and sulfidation reactions have been removed from the gas generation model (Section MASS-5.2). The Repository Fluid Flow conceptual model represents the long-term flow behavior of liquid and gas in the repository and its interaction with other regions in which fluid flow may occur, such as the Salado, shafts, or an intrusion borehole. This model is not used to represent the interaction of fluids in the repository with a borehole during drilling. Historical information on alternative conceptual models for brine inflow to the repository is contained in the CCA, Appendix MASS, Section MASS-7.0.

The first principle in the conceptual model for fluid flow in the repository is that gas and brine can both be present and mobile (two-phase flow), governed by conservation of energy and mass and by Darcy's Law for their fluxes (see Appendix PA-2019, Section PA-4.2). Consistent with typical concepts of two-phase flow, the phases can affect each other by impeding flow caused by partial saturation (relative permeability effects) and by affecting pressure caused by capillary forces (capillary pressure effects).

The flow of brine and gas in the repository is assumed to behave as two-phase, immiscible, Darcy flow (see Appendix PA-2019, Section PA-4.2). BRAGFLO is used to simulate brine and gas flow in the repository and to incorporate the effects of disposal-room closure and gas generation. Fluid flow in the repository is affected by the following factors:

- The geometric association of pillars, rooms, and drifts; waste panel consolidation due to salt creep; and possible borehole locations
- The varied properties of the waste areas resulting from creep closure and heterogeneous contents
- Flow interactions with other parts of the disposal system
- Reactions that generate gas

The geometry of the panel around the intrusion borehole is consistent with the assumption that the fluid flow there will occur directly toward or directly away from the borehole. The geometry represents a semicircular volume north of the borehole and a semicircular volume south of the borehole (representing radial flow in a subregion of a two-dimensional representation of the repository).

Approximating convergent and divergent flow around the intrusion borehole creates a narrow neck in the otherwise fairly uniform numerical grid in the region representing the repository. In the undisturbed performance scenario, and under certain conditions in other scenarios, flow in the repository may pass laterally through this neck. In reality, this neck does not exist. Its presence in the model is expected to have a negligible or conservative impact on model predictions compared to predictions that would result from a more realistic model geometry. The time scale involved and the permeability contrast between the repository and surrounding rock are sufficient so that the lateral flow that may occur in the repository is restricted by the rate at which liquid gets into or out of the repository, rather than by the rate at which it flows through the repository.

Gas generation is affected by the quantity of liquid in contact with metal and CPR waste materials and radionuclides in the waste for the case of radiolytic gas generation. However, the distribution of fluid in the repository can only be approximated. For example, capillary action can create wicking that would increase the overall region in which gas generation occurs, but modeling this at the necessary resolution to simulate these processes would greatly increase the time required to carry out the modeling (Appendix PA-2019, Section PA-4.2.6, and CRA-2004, Section 6.4.3.3). Therefore, as a bounding measure for gas generation purposes, brine in the repository is distributed to an extent greater than estimated by the Darcy flow models or by the values of parameters chosen.

Modeling of flow within the repository is based on homogenizing the room contents into relatively large computational volumes. The approach ignores heterogeneities in disposal room contents that may influence gas and brine behavior by causing fluid flow among channels or creating preferential paths in the waste, bypassing entire regions. Isolated regions could exist for several reasons:

- They may be isolated by low-permeability regions of waste that serve as barriers.
- Connectivity with the interbeds may occur only at particular locations within the repository.
- The repository dip may promote preferential gas flow in the upper regions of the waste.

For the CCA, the adequacy of the repository homogeneity assumption was examined in screening analyses DR-1 (Webb 1995) and DR-6 (Vaughn, Lord, and MacKinnon 1995a). These analyses used an additional parameter in BRAGFLO to specify the minimum active (mobile) brine flow saturation (pseudoresidual brine saturation). Above this saturation, the normal descriptions of two-phase flow apply (i.e., either the Brooks and Corey or van Genuchten and Parker relative permeability models). Below this minimum, brine is immobile, although it is available for reaction and may still be consumed during gas-generation reactions. The assumption of a minimum saturation limit was justified based on the presumed heterogeneity of the waste and the slight dip in the repository. The minimum active brine saturation was treated as an uncertain parameter and sampled uniformly between the values 0.1 and 0.8 during the analysis. This saturation limit was applied uniformly throughout the disposal room to bound the impact of heterogeneities on flow (Webb 1995; Vaughn, Lord, and MacKinnon 1995a). Results of this analysis showed that releases to the accessible environment in the baseline case (homogenization) are consistently higher.

The EXP and OPS regions were represented in the CCA PA by a fixed porosity of 18.0% and a permeability of 10^{-11} m^2. The combination of low porosity and high permeability conservatively overestimated fluid flow through these regions and limited the capacity of these regions to store fluids, potentially overestimating releases to the environment. This conclusion was based on a screening analysis (Vaughn, Lord, and MacKinnon 1995b) that examined the importance of permeability varying with porosity in closure regions (waste disposal region, EXP region, and OPS region). To perform this analysis, a model for estimating the change in permeability with porosity in the closure regions was implemented in BRAGFLO. A series of BRAGFLO simulations was performed to determine whether permeability varying with porosity in the closure regions could enhance contaminant migration to the accessible environment. Two basic scenarios were considered in the screening analysis: undisturbed performance and disturbed performance. To assess the sensitivity of system performance on dynamic permeability in the closure regions, CCDFs of normalized contaminated brine releases were constructed and compared with the corresponding baseline conditional CCDFs. The baseline model treated permeabilities in the closure regions as fixed values. Results of this analysis showed that the inclusion of dynamic closure of the waste disposal region, EXP region, and OPS region in BRAGFLO resulted in computed releases to the accessible environment that are essentially equivalent to the baseline case.

A separate analysis (Park and Hansen 2003) examined the possible effects of heterogeneity in waste container and waste material strength on room closure. The analysis of room closure found that the room porosity may vary widely depending on the type of waste container and the emplacement of waste in the repository. However, analysis of a separate PA (Hansen et al. 2003) found that PA results are relatively insensitive to the uncertainty in room closure and room porosity. The conclusions of the separate PA are summarized in Section MASS-18.0.

MASS-5.1 Flow Interactions with the Creep Closure Model

Flow interactions with the creep closure model implemented in WIPP PA have not changed since the CRA-2014 PA. The dynamic effect of halite creep and room consolidation on room porosity is modeled only in the waste disposal region. Other parts of the repository, such as the open panel closure areas, EXP region, and the OPS region, are modeled assuming fixed (invariant with time) properties. In these regions, the permeability is held at a relatively high fixed value representative of unconsolidated material, while the porosity is maintained at relatively low values associated with highly consolidated material. This combination of low porosity and high permeability is assumed to conservatively overestimate flow through these regions and minimize the capacity of this material to store fluids, thus maximizing the release to the environment. To examine the acceptability of this assumption, a screening analysis (Vaughn, Lord, and MacKinnon 1995c) evaluated the effect of including closure of the EXP region and OPS region. In this analysis, consolidation of the EXP region and OPS region was implemented in BRAGFLO by relating pressure and time to porosity using a porosity-surface method. The porosity surface for the EXP region and OPS region differs from the surface used for consolidation of the disposal room and is based on an empty excavation (see Appendix PORSURF-2014). The screening analysis showed that disregarding dynamic closure of the EXP region is acceptable because it is conservative: lower releases occur when closure of the EXP region and OPS region is computed compared to simulations with time-invariant high

permeability and low porosity. The creep closure of open panel closure areas is treated in the same manner as that for the OPS and EXP regions (Zeitler et al. 2017).

MASS-5.2 Flow Interactions with the Gas Generation Model

Three changes have been made to the gas generation model implemented in WIPP PA since the CRA-2014 PA: Section 1) the addition of brine radiolysis as a gas generation mechanism; 2) the removal of reaction of iron hydroxide with hydrogen sulfide; and 3) the addition of the possibility of no conversion of hydromagnesite to magnesite.

Gas generation affects repository pressure, which in turn is an important parameter in other processes such as two-phase flow, creep closure, and fracturing of the interbeds and DRZ. Gas-generation processes considered in PA calculations include radiolytic gas generation, anoxic corrosion, and microbial degradation. Prior to the CRA-2019 PA, radiolysis was excluded from PA calculations on the basis of laboratory experiments and a screening analysis (Vaughn, Lord, MacKinnon 1995d) that concluded that radiolysis does not significantly affect repository performance. However, an updated screening analysis concluded that radiolysis does substantially impact repository performance and thus radiolytic gas generation has been added to the gas generation model for the CRA-2019 PA (Day 2019).

In modeling anoxic corrosion and microbial degradation gas generation, the effective liquid in a computational cell is the computed liquid in that cell plus an adjustment for the uncertainty associated with wicking by the waste (see Appendix PA-2019, Section PA-4.2.6). Capillary action (wicking) is the ability of a material to carry a fluid by capillary forces above the level it would normally seek in response to gravity. Because the current gas-generation model computes substantially different gas-generation rates depending on whether the waste is wet or merely surrounded by water vapor, the physical extent of wetting could be important. A screening analysis (Vaughn, Lord, and MacKinnon 1995d) examined wicking and concluded that it should be included in PA calculations.

The baseline gas-generation model in BRAGFLO accounts for corrosion of iron, microbial degradation of cellulose and possibly plastics and rubber, and radiolysis of brine. The net reaction rates of corrosion of iron and microbial degradation of cellulose and possibly plastics and rubber depend directly on brine saturation: an increase in brine saturation will increase the net reaction rate by weighting the inundated portion more heavily and the slower humid portion less heavily.[2] To simulate the effect of wicking on the net reaction rate, an effective brine saturation, which includes a wicking saturation contribution, is used to calculate reaction rates rather than the actual brine saturation (see Appendix PA-2019, Section PA-4.2.6). The radiolytic gas generation rate also depends on brine saturation, but no associated humid rate is assumed and there is no impact of wicking on the reaction rate. Dissolved radionuclides and a variable fraction of wetted solid radionuclides contribute to this process (see Appendix PA-2019, Section PA-1.1).

Additional gas and brine production and consumption reactions exist in the overall flow model. As described in the Chemical Conditions Conceptual Model (U.S. DOE 2004, sections PEER-

[2] In the CRA-2019 PA, an updated range of inundated steel corrosion rates (Zeitler 2018a) was used and nonzero values of humid steel corrosion rates (Zeitler 2018b) were used for the first time.

2004 1.1.3, PEER-2004 1.1.4 and PEER-2004 1.1.5), the major reactions in the repository include the reactions of CPR, iron, and MgO with brine. The generation of water in these pathways is also considered. The reaction of iron hydroxide with hydrogen sulfide, which consumes gas and produces water, was included in the CRA-2014 PA, but not in the CRA-2019 PA as the passivation of steel by H_2S is no longer considered a valid assumption (Appendix GEOCHEM-2019, Section GEOCHEM-2.1.6). MgO reactions also include MgO hydration, which consumes water and produces brucite, and the carbonation of brucite, which is assumed to form hydromagnesite. It is assumed that the carbon dioxide preferentially reacts with the brucite versus the dry MgO. The reaction of hydromagnesite to form magnesite and water is also included. An updated range of hydromagnesite conversion rates was used in the CRA-2019 PA (Zeitler 2019c) and includes the possibility of no conversion to magnesite via a lower rate bound of zero. All chemical reactions and species are tracked on a cell-by-cell basis. There is a finite amount of each chemical species in each cell. Once any of them are used up, that particular reaction ceases. The reactions that comprise the repository water balance implementation are more fully discussed in Appendix GEOCHEM-2019, Section GEOCHEM-2.2.

MASS-6.0 Gas Generation

The gas generation model represents the possible generation of gas in the repository by radiolysis of brine, corrosion of steel, and microbial degradation of CPR materials. The CRA-2014 PA used the CRA-2004 PABC gas generation modeling assumptions, which did not include the radiolysis of brine. Brine radiolysis has been shown to be a potentially substantial source of gas generation that can impact repository pressure and brine saturation conditions in the repository (Day 2019). It has been added to the gas generation model for the CRA-2019 PA (Section MASS-6.1, Appendix GEOCHEM, Section GEOCHEM-2.1, and Appendix PA-2019, Section PA-1.1).

Additional discussion of gas generation may be found in Appendix GEOCHEM-2019, Section GEOCHEM-2.1, Appendix PA-2019, Section PA-4.2.5 and the CRA-2004, Chapter 6.0, Section 6.4.3.3. See the CCA, Appendix MASS, Section MASS-8.1 for historical information on the development of the CCA gas-generation conceptual model.

MASS-6.1 Addition of Radiolysis to Gas Generation Modeling for CRA-2019

Gas generation due to radiolysis of brine from radionuclides in solution and in wetted-solid form was included in gas generation modeling for the CRA-2019 PA. Gas generation due to radiolysis of CPR was not included in the gas generation model, based on the process not having a significant impact on the performance of the repository due to matrix depletion (Day 2019).

Day (2019) also described the following assumptions related to brine radiolysis:

1. For the purposes of WIPP PA, the radiolysis of brine can be considered to result in only the production of hydrogen gas and not oxygen gas due to its reaction with metals in the waste (i.e., one mole of gas produced for each net mole of water consumed).

2. In WIPP, the inventory of alpha-emitting radionuclides is sufficiently large, and the solubility coefficients and brine volumes are sufficiently small, such that only a small

fraction of the total alpha-emitting inventory can be dissolved. Although not dissolved, the remaining solid alpha-emitting radionuclide inventory in close-proximity to brine can also contribute to radiolytic gas generation. The amount of each radionuclide contributing to radiolysis is from the amount of each radionuclide in solution and the remaining amount of each radionuclide in solid form that is wetted by brine.

3. Only a portion of the disintegration energy associated with wetted-solid alpha-emitting radionuclides in the inventory will contribute to radiolytic H_2 generation due to several factors, including particle size, self-attenuation, and proximity of the radionuclide particle to brine and other attenuating substrates.

4. The total radiolytic H_2 generation rate (and brine consumption rate) is due to contributions from one or more decaying radionuclides in the waste volume.

MASS-7.0 Chemical Conditions

The modeling assumptions of chemical conditions used in the CRA-2019 PA are changed from those used in the CRA-2014 PA to include aqueous lead and iron (Appendix GEOCHEM-2019, Section GEOCHEM-3.5). The models used for chemical conditions in the repository are discussed in Appendix SOTERM-2019, Section SOTERM-6.6 and Appendix GEOCHEM-2019, Section GEOCHEM-3.2.

MASS-8.0 Dissolved Actinide Source Term

The dissolved An source term modeling assumptions used in the CRA-2019 remain unchanged from those used in the CRA-2014 PA, but some model parameters are updated for the CRA-2019 PA. The models used for the dissolved An source term in the repository are discussed in Appendix SOTERM-2019, Section SOTERM-6.0 and Appendix PA-2019, Section 4.4.

MASS-9.0 Colloidal Actinide Source Term

The colloidal An source term modeling assumptions used in the CRA-2019 were unchanged since the CCA but some model parameters were updated for the CRA-2019 (Reed, Swanson, and Stanley 2019). The models used for the colloidal An source, and An source term updates included in the CRA-2019 PA, are discussed in Appendix GEOCHEM-2019, Section 5.4, Appendix SOTERM-2019, Section 3.5, and Appendix PA-2019, Section 4.4.

MASS-10.0 Shafts and Shaft Seals

The shafts and shaft seals modeling assumptions used in the CRA-2019 have changed from those used in the CRA-2014 PA, with the incorporation of a fifth shaft into the combined shaft representation in the BRAGFLO grid (Zeitler 2019b). Shaft properties have not been changed in the CRA-2019 PA. The models used for shafts and shaft seals are discussed in Appendix PA-2004, Attachment MASS, Section MASS-12.0, and Appendix PA-2019, Section PA-4.2.7.

MASS-11.0 Salado

The far-field Salado modeling assumptions used in the CRA-2019 remain unchanged from those used in the CRA-2014 PA apart from two minor changes: 1) the MB representation that existed above and below the southernmost panel closure in the CRA-2014 PA BRAGFLO grid has been removed along with the "panel closure DRZ" (Section MASS-11.3); and 2) the number of time steps over which BRAGFLO results are averaged for input into the NUTS code has decreased from 20 to 5 (Section MASS-11.4). The purpose of this model is to reasonably represent the effects of fluid flow in the Salado on long-term performance of the disposal system. The conceptual model is also discussed in the CRA-2004, Chapter 6.0, Section 6.4.5.

Fluid flow in the Salado is considered in the conceptual model of long-term disposal system performance for several reasons. First, some liquid could move from the Salado to the repository because of the considerable gradients that can form for liquid flow inward to the repository. This possibility is important because such fluid can affect creep closure, gas generation, An solubility, and other processes occurring in the repository. Second, gas generated in the repository is thought to be capable of fracturing the Salado interbeds under certain conditions, creating increased permeability channels that could be pathways for lateral transport. The lateral transport pathway in intact Salado is also modeled, but it is considered unlikely to result in any significant radionuclide transport to the accessible environment boundary.

The fundamental principle in the conceptual model for fluid flow in the Salado is that it is a porous medium within which gas and brine can both be present and mobile (two-phase flow), governed by conservation of energy and mass and by Darcy's Law for their fluxes (see Appendix PA-2019, Sections PA-4.2). Consistent with typical concepts of two-phase flow, each phase can affect the other by impeding flow because of partial saturation (relative permeability effects) and by affecting pressure by capillary forces (capillary pressure effects). It was originally assumed that no waste-generated gas is present before repository closure. However, during the EPA completeness review of the CRA-2004, the representation of the gas-generation rate was changed for the CRA-2004 PABC (Cotsworth 2005). The repository was precharged after closure to represent the short-term, but initially faster, microbial gas-generation rate (see Leigh et al. 2005, Section 2.3). Future states are modeled as producing gas by corrosion, microbial activities, and brine radiolysis. Should high pressure develop over the regulatory period, it is allowed to access MBs in the Salado.

Some variability in composition exists between different horizons of the Salado. The largest differences occur between the anhydrite-rich layers called interbeds and those dominated by halite. Within horizons dominated by halite, composition varies from nearly pure halite to halite plus several percent other minerals, in some instances including clay (see the CCA, Chapter 2.0, Section 2.1.3.4). The Salado is modeled as impure halite except for those interbeds that intersect the DRZ near the repository. This conceptual model and an alternative model that explicitly represented all stratigraphically distinct layers of the Salado near the repository (Christian-Frear and Webb 1996) produced similar results.

From other modeling and theoretical considerations, flow between the Salado and the repository is expected to occur primarily through interbeds that intersect the DRZ. Because of the large surface areas between the interbeds and surrounding halite, the interbeds serve as conduits for

the flow of brine in two directions: from halite to interbeds to the repository or, for brine flowing out of the repository, from the repository into interbeds and then into halite. Because the repository is modeled as a relatively porous and permeable region, brine is considered most likely (but not constrained) to leave the repository through MB 139 below the repository because of the effect of gravity. If repository pressures become sufficiently high, gas is modeled to exit the repository via the MBs.

The effect of gravity may also be important in the Salado because of the slight and variable natural stratigraphic dip. For long-term performance modeling, the dip in the Salado within the domain is taken to be constant and 1 degree from north to south.

Fluid flow in the Salado is conceptualized as occurring either convergently into the repository or divergently from it, as discussed in detail in the CRA-2004, Chapter 6.0, Section 6.4.2.1. Because the repository is not conceptualized as homogeneous, implementing a geometry for the conceptual model of convergent or divergent flow in the Salado is somewhat complicated and is discussed in the CRA-2004, Chapter 6.0, Section 6.4.2.1.

The conceptual model for Salado fluid flow has primary interactions with three other conceptual models. The interbed fracture conceptual model allows porosity and permeability of the interbeds to increase as a function of pressure. The repository fluid flow model is directly coupled to the Salado fluid flow model by the governing equations of flow in BRAGFLO (in the governing equations of the mathematical model, they cannot be distinguished), and it differs only in the region modeled and the parameters assigned to materials. The Salado model for An transport is directly coupled to the conceptual model for flow in the Salado through the process of advection. Additional information on the treatment of the Salado in PA is found in Appendix PA-2019, Section PA-4.2.

MASS-11.1 High Threshold Pressure for Halite-Rich Salado Rock Units

The assumptions regarding the threshold pressure in the Salado in WIPP PA have not changed since the CRA-2014 PA. An important parameter used to describe the effects of two-phase flow is threshold pressure, which helps to determine the ease with which gas can enter a liquid-saturated rock unit. For a brine-saturated rock, the threshold pressure is defined as “equal to the capillary pressure at which the relative permeability to the gas phase begins to rise from its zero value, corresponding to the incipient development of interconnected gas flow paths through the pore network” (Davies 1991, p. 9).

The threshold pressure, as well as other parameters used to describe two-phase characteristics, has not been measured for halite-rich rocks of the Salado. The Salado, however, is thought to be similar in pore structure to rocks for which threshold pressures have been measured (Davies 1991). Based on this observation, Davies (Davies 1991) postulated that the threshold pressure of the halite-rich rocks in the Salado could be estimated if an empirical correlation exists between rocks postulated to have similar pore structure.

Davies developed a correlation between threshold pressure and intrinsic permeability applicable to the Salado halites. A similar correlation was developed for Salado anhydrites; subsequent testing confirmed that the correlation predicted threshold pressures accurately. The correlation

developed by Davies predicts threshold pressures in intact Salado halites on the order of 20 megapascals (MPa) or greater (Davies 1991). This threshold pressure predicted by correlation is much higher than that expected to persist in the repository, so that for all practical and predictive purposes, no gas will flow into intact Salado halites (see the CRA-2004, Chapter 6.0, Section 6.4.5.1).

Because threshold pressure helps control the flow of gas, and because the greatest volume of rock in the Salado is rich in halite, a high threshold pressure effectively limits the volume of gas that can be accommodated in the pore spaces of the intact host formation. Thus, high threshold pressure is considered conservative, because if gas could flow into the pore spaces of intact Salado halite, repository pressures could be reduced dramatically.

See the CCA, Appendix MASS, Section MASS-13.2 for the historical information relating to the CCA Salado conceptual model. The Salado conceptual model is unchanged for the CRA-2019 PA.

MASS-11.2 The Fracture Model

The assumptions regarding the fracture model implemented in WIPP PA have not changed since the CRA-2014 PA. The purpose of this model is to alter the porosity and permeability of the anhydrite interbeds and the DRZ if their pressure approaches lithostatic, simulating some of the hydraulic effects of fractures with the intent that unrealistically high pressures (in excess of lithostatic) do not occur in the repository or disposal system. The conceptual model is also discussed in the CRA-2004, Chapter 6.0, Section 6.4.5.2.

In the 1992 preliminary PA, repository pressures were shown to greatly exceed lithostatic pressure (14.8 MPa) if a large quantity of gas was generated. Pressures within the waste repository and surrounding regions were predicted to be roughly 20 to 25 MPa. It is expected that fracturing within the anhydrite MBs would occur at pressures slightly above lithostatic pressure, and this fracturing is implemented through a pressure-dependent compressibility.

Two parametric behaviors must be quantified in the conceptual model. First, the change of porosity with pressure in the anhydrite MBs must be specified. This is done with a relatively simple equation, described in Appendix PA-2019, Section PA-4.2.4, that relates porosity change to pressure change using an assumption that the fracturing can be thought of as increasing the compressibility of interbeds. Parameters in the model are treated as fitting parameters and have little relation to physical behavior except that they affect the porosity change. The second parametric behavior is the change of permeability with pressure, which is incorporated by a functional dependence on the porosity change. It is assumed that a power function is appropriate for relating the magnitude of permeability increase to the magnitude of porosity increase. The parameter in this power function, an exponent, is also treated as a fitting parameter and can be set so that the behavior of permeability increase with porosity increase fits the desired behavior.

The one-degree dip modeled in BRAGFLO may affect fracture propagation direction; however, within the accuracy of the finite difference grid, a fracture will develop radially outward. This would not account for fracture fingering or a preferential fracturing direction; however, no existing evidence supports heterogeneous anhydrite properties that would contribute to

preferential fracture propagation. This evidence is discussed in the CCA, Appendix MASS, Attachment 13-2.

The maximum enhanced fracture porosity controls the storativity within the fracture. The extent of the migration of the gas front into the MB is sensitive to this storativity. The additional storativity caused by porosity enhancement will mitigate gas migration within the MB. The enhancement of permeability by MB fracturing will make the gas more mobile and will contribute to longer gas-migration distances. Thus, the effects of porosity enhancement at least partially counteract the effects of permeability enhancement in affecting the gas-migration distances.

Because intact anhydrite is partially fractured, the pressure at which porosity or permeability changes are initiated is close to the initial pressure within the anhydrite. The fracture treatment within the MBs will not contribute to early brine drainage from the MB because the pressures at these times are below the fracture initiation pressure.

The input data to the interbed fracture model (Kim and Feng 2019) were chosen deterministically to produce the appropriate pressure and porosity response as predicted by a linear elastic fracture mechanics model, as discussed in Mendenhall and Gerstle (Mendenhall and Gerstle 1993).

MASS-11.3 Flow in the DRZ

The CRA-2019 PA modeling assumptions for flow in the salt DRZ remain unchanged from those used in the CRA-2014 PA. The conceptual model for the DRZ around the waste disposal, OPS, and EXP regions has been chosen to provide a reasonably conservative estimate of fluid flow between the repository and the intact halite and anhydrite MBs. The conceptual model is also discussed in the CRA-2004, Chapter 6.0, Section 6.4.5.3.

The conceptual model implemented in the CCA PA used values for the permeability and porosity of the salt DRZ that did not vary with time. A screening analysis examined an alternative conceptual model for the DRZ in which permeability and porosity changed dynamically in response to changes in pressure (Vaughn, Lord, and MacKinnon 1995e). This analysis implemented a fracturing model in BRAGFLO for the salt DRZ. This fracturing model is used in the existing anhydrite interbed model. In this model, formation permeability and porosity depend on brine pressure, as described by Freeze, Larsen, and Davies (Freeze, Larsen, and Davies 1995, pp. 2-16 through 2-19) and Appendix PA-2019, Section PA-4.2.4. This model permits the representation of two important formation-alteration effects. First, pressure buildup caused by gas generation and creep closure within the waste will slightly increase porosity within the DRZ and offer additional fluid storage with lower pressures. Second, the accompanying increase in formation permeability will enhance fluid flow away from the DRZ. An increase in porosity tends to reduce outflow into the far field. As a result, parameter values for this analysis were selected so that the DRZ alteration model greatly increases permeability while only modestly increasing porosity.

Two basic scenarios were considered in the screening analysis by Vaughn, Lord, and MacKinnon (Vaughn, Lord, and MacKinnon 1995e): undisturbed repository performance and disturbed repository performance. Both scenarios included a one-degree formation dip

downward to the south. Intrusion event E1 is considered in the disturbed scenario and consists of a borehole that penetrates the repository and pressurized brine in the underlying Castile. Two variations of intrusion event E1 were examined: E1 updip and E1 downdip. In the E1 updip event, the intruded panel region was located on the north end of the waste disposal region, whereas in the E1 downdip event, the intruded panel region was located on the south end of the disposal region. These two different geometries permitted evaluation of the possibility of increased brine flow into the panel region and the potential for subsequent impacts on contaminant migration. To incorporate the effects of uncertainty in each case (E1 updip, E1 downdip, and undisturbed), a Latin hypercube sample (LHS) size of 20 was used, for a total of 60 simulations. To assess the sensitivity of system performance on formation alteration of the DRZ, conditional CCDFs of normalized contaminated brine releases were constructed and compared with the corresponding baseline model conditional CCDFs that were computed with constant DRZ permeability and porosity values. Based on comparisons between conditional CCDFs, computed releases to the accessible environment were determined to be essentially equivalent between the two treatments. Since the two configurations were determined to have essentially equivalent impacts on releases, the intrusion borehole was assumed to intrude in the down-dip or south side of the repository where it is assumed brine would more readily accumulate (see Figure MASS-1).

Preliminary PAs considered alternative conceptual models that allowed for some lateral extent of the DRZ into the halite surrounding the waste disposal region and for the development of a transition zone between anhydrites A and B and MB 138 (WIPP Performance Assessment 1993, Volume 4, Figure 4.1-2 and Figure 5.1-2; Davies, Webb, and Gorham 1992; Gorham et al. 1992). The transition zone was envisioned as a region that had experienced some hydraulic depressurization and perhaps some elastic stress relief because of the excavation, but probably no irreversible rock damage and no large permeability changes. Modeling results indicated that including the lateral extent of the DRZ had no significant effect on fluid flow. Communication vertically to MB 138 was thought to be a potentially important process, however, and the model adopted for PA assumes that the DRZ extends upward to MB 138 and permeability is sampled over the same range used in the CCA Performance Assessment Verification Test (PAVT). This representation continues to be used in the CRA-2019 PA. One minor change to the modeling implementation of the DRZ-MB interface is that the MB representation that existed above and below the southernmost panel closure in the CRA-2014 PA BRAGFLO grid has been removed along with the “panel closure DRZ” for consistency in treating the DRZ above open areas, now that the southernmost panel closure area is modeled as not having ROMPCS properties in the CRA-2019 PA (Figure MASS-1, Zeitler 2019a).

MASS-11.4 Actinide Transport in the Salado

The An transport modeling assumptions used in the CRA-2019 PA remain unchanged from those used in the CRA-2014 PA. The purpose of this model, implemented in the code NUTS, is to represent the transport of An in the Salado. This model is also discussed in the CRA-2004, Chapter 6.0, Section 6.4.5.4, and Appendix PA-2019, Section PA-4.3.4.

An transport in the Salado is conceptualized as occurring only by advection, or movement of material through the bulk flow of a fluid, through the porous medium described in the Salado hydrology conceptual model. Advection is a direct function of fluid flow, which is discussed in

the conceptual model for Salado fluid flow. Other processes that might disperse An, such as diffusion, hydrodynamic dispersion, and channeling in discrete fractures, are not included in the conceptual model. Since these processes will reduce An transport, it is conservative to ignore these processes.

To model radionuclide transport in the Salado, NUTS takes as input BRAGFLO's velocity field, pressures, porosities, saturations, and other model parameters (including geometrical grid, residual saturation, material map, brine compressibility, and time step) averaged over a given number of time steps (5 for the CRA-2019 PA calculations). NUTS then models the transport of radionuclides within all the regions for which BRAGFLO computes brine and gas flow. The brine must pass through some part of the repository at some point during the 10,000-year regulatory period if it is to become contaminated. Radioactive constituents of the waste in the repository are assumed to dissolve into the brine while the brine is in the repository; the radionuclides are then transported by advection to other regions outside the repository. Consequently, the results of NUTS are subject to all the uncertainties associated with BRAGFLO's conceptual model and parameterization. Details of the source term, which specifies the types and amounts of radionuclides that are assumed to come into contact with the waste, are discussed in Appendix PA-2019, Section 4.4.

NUTS neglects molecular dispersion. For materials of interest in the WIPP repository system, molecular diffusion coefficients are, at most, on the order of 4×10^{-10} m^2 per second. Thus, the simplest scaling argument using a time scale of 10,000 years leads to a molecular diffusion (that is, mixing) length scale of approximately 10 m (33 ft), which is negligible compared to the lateral advection length scale of roughly 2,400 m (7,874 ft) (the lateral distance from the repository to the accessible environment).

NUTS also neglects mechanical dispersion (see the CRA-2004, Chapter 6.0, Section 6.4.5.4.2). Dispersion is quantified by dispersivities, which are empirical tensor factors proportional to flow velocity (to within geometrical factors related to flow direction). They account for both the downstream and cross-stream spreading of local extreme values in concentration of dissolved constituents. Physically, the spreading is caused by the fact that both the particle paths and velocity histories of once-neighboring particles can be vastly different because of material heterogeneities characterized by permeability variations. These variations arise from the irregular cross-sectional areas and tortuous inhomogeneous, anisotropic connectivity between pores. Because of its velocity dependence, the transverse component of mechanical dispersivity tends to transport dissolved constituents from regions of relatively rapid flow (where mechanical dispersion has a larger effect) to regions of slower flow (where mechanical dispersion has a smaller effect). In the downstream direction, dispersivity merely spreads constituents in the flow direction. Conceptually, ignoring lateral spreading assures that dissolved constituents will remain in the rapid part of the flow field, which assures their transport toward the boundary. Similarly, ignoring longitudinal dispersivity ignores the elongation of a feature in the flow direction, which would delay the arrival of radionuclide constituents at the accessible environment. However, because the EPA release limits are time-integrated measures, the exact time of arrival is unimportant for constituents that arrive at the accessible environment, so long as arrival occurs within the assessment period (10,000 years).

NUTS conservatively disregards sorptive and other retarding effects throughout the entire flow region even though retardation must occur at some level within the repository, the MBs, and the anhydrite interbeds, and especially in zones with clay layers or clay as accessory minerals. Advection is, therefore, the only transport mechanism considered in NUTS. Because the Darcy flows are given by BRAGFLO to NUTS as input, the maximum solubility limits for combined dissolved and colloidal components are the most important NUTS parameters. These components are described in Appendix PA-2019, Section 4.4.

MASS-12.0 Geologic Units above the Salado

The modeling assumptions of the geologic units above the Salado used in the CRA-2019 PA remain unchanged from those used in the CRA-2014 PA. The model for geologic units above the Salado was developed to provide a reasonable and realistic basis for simulations of fluid flow within the disposal system and detailed simulations of groundwater flow and radionuclide transport in the Culebra. The conceptual model for these units is also discussed in the CRA-2004, Chapter 6.0, Section 6.4.6.

The conceptual model used in PA for the geologic units above the Salado is based on the overall concept of a groundwater basin, as introduced in the CRA-2004, Chapter 2.0, Section 2.2.1.1, and in the CCA, Appendix MASS, Section MASS-14.2. The computer code SECOFL3D was originally used to evaluate the effect on regional-scale fluid flow by recharge and rock properties in the groundwater basin above the Salado (see the CCA, Appendix MASS, Attachment 17-2). However, simpler models for this region are implemented in codes used in PA. For example, in the BRAGFLO model, layer thicknesses, important material properties including porosity and permeability, and hydrologic properties such as pressure and initial fluid saturation are specified, but the model geometry and boundary conditions are not suited to groundwater basin modeling (nor is the BRAGFLO model used to make inferences about groundwater flow in the units above the Salado). In PA, the Culebra is the only subsurface pathway modeled for radionuclide transport above the Salado, although the groundwater basin conceptual model includes other flow interactions. The Culebra model implemented in PA includes spatial variability in hydraulic conductivity and uncertainty and variability in physical and chemical transport processes. Thus, the geometries and properties of units in the different models applied to the units above the Salado by the DOE are chosen to be consistent with the purpose of the model.

The MODFLOW-2000 and SECOTP2D codes are used directly in PA to model fluid flow and transport in the Culebra. The assumptions made in these codes are discussed in the CRA-2004, Chapter 6.0, Section 6.4.6.2, and Appendix PA-2004, Attachment MASS, Section MASS-15.0.

With respect to the units above the Salado, the BRAGFLO model is used only for determination of fluid fluxes between the shaft or intrusion borehole and hydrostratigraphic units. For this purpose, it does not need to resolve regional or local flow characteristics.

The basic stratigraphy and hydrology of the units above the Salado are described in the CRA-2004, Chapter 2.0, Section 2.1.3.5, Section 2.1.3.6, Section 2.1.3.7, Section 2.1.3.8, Section 2.1.3.9, Section 2.1.3.10, and Section 2.2.1.4. Additional supporting information is contained in the CCA, Appendices GCR, HYDRO, and SUM. Details of the conceptual model for each unit are described in the CRA-2004, Chapter 6.0, Section 6.4.6.1, Section 6.4.6.2, Section 6.4.6.3,

Section 6.4.6.4, Section 6.4.6.5, Section 6.4.6.6, and Section 6.4.6.7, and additional information on units above the Salado is found in Appendix HYDRO-2014.

See the CCA, Appendix MASS, Section MASS-14.1 for historical information relating to the conceptual models for units above the Salado for the CCA. The conceptual models for the units above the Salado are unchanged for CRA-2019 PA.

MASS-12.1 Groundwater-Basin Conceptual Model

The groundwater-basin conceptual model and associated modeling assumptions used in the CRA-2019 PA remain unchanged from those used in the CRA-2014 PA. For a discussion on the groundwater-basin conceptual model, see the CCA, Appendix MASS, Section MASS-14.2.

MASS-13.0 Flow through the Culebra

The Culebra flow modeling assumptions used in the CRA-2019 PA remain unchanged from those used in the CRA-2014 PA. The conceptual model for groundwater flow in the Culebra (1) provides a reasonable and realistic basis for simulating radionuclide transport in the Culebra, and (2) allows evaluation of the extent to which uncertainty about groundwater flow in the Culebra may contribute to uncertainty in the estimate of cumulative radionuclide releases from the disposal system. See the CRA-2004, Chapter 6.0, Section 6.4.6.2 for additional references to other relevant discussions on this conceptual model.

The conceptual model used in PA for groundwater flow in the Culebra treats the Culebra as a confined two-dimensional aquifer with constant thickness and spatially varying transmissivity (see the CCA, Appendix MASS, Attachment 15-7). Flow is modeled as single-phase (liquid) Darcy flow in a porous medium.

Basic stratigraphy and hydrology of the units above the Salado are described in the CRA-2004, Chapter 2.0, Section 2.1 and Section 2.2. Additional supporting information is contained in the CCA, Appendices GCR, HYDRO, and SUM.

The conceptual model for flow in the Culebra is discussed in the CRA-2004, Chapter 6.0, Section 6.4.6.2. Details of the calibration of the T fields, based on available field data, are given in Appendix TFIELD-2014. Initial and boundary conditions used in the model are given in the CRA-2004, Chapter 6.0, Section 6.4.10.2. A discussion of the adequacy of the two-dimensional assumption for PA calculations is included in the CCA, Appendix MASS, Attachment 15-7.

The principal parameter used in PA to characterize flow in the Culebra is an index parameter (the transmissivity index) used to select a single T field for each LHS element from a set of calibrated fields (see Kim and Feng 2019, Table 1), each of which is consistent with available data.

See Appendix PA-2004, Attachment MASS, Section MASS-15.1 for historical information relating to the Culebra conceptual model. The conceptual model for this unit is unchanged for the CRA-2019 PA.

MASS-13.1 Dissolved Actinide Transport and Retardation in the Culebra

The purpose of this model is to represent the effects of advective transport and physical and chemical retardation on the movement of An in the Culebra. This conceptual model is also discussed in the CRA-2004, Chapter 6.0, Section 6.4.6.2.1. No changes have been made to this model since the CRA-2014 PA. For a historical presentation of this model, see Appendix PA-2004, Attachment MASS, Section MASS-15.2.

MASS-13.2 Colloidal Actinide Transport and Retardation in the Culebra

The purpose of this model is to represent the effects of colloidal An transport in the Culebra. This model is also discussed in the CRA-2004, Chapter 6.0, Section 6.4.6.2.2 and Appendix PA-2004, Attachment MASS, Attachments 15-2, 15-8, and 15-9. No changes have been made to this model since the CRA-2014 PA. Additional information and historical information on colloidal An transport and retardation in the Culebra can be found in Appendix PA-2004, Attachment MASS, Section MASS-15.3.

MASS-13.3 Subsidence Caused by Potash Mining in the Culebra

The mining-related modeling assumptions used in the CRA-2019 PA remain unchanged from those used in the CRA-2014 PA. This model incorporates the effects of potash mining in the McNutt Potash Zone on disposal system performance (see Appendix SCR-2014, FEP H13, FEP H37, and FEP H38). Provisions in Part 194 provide a conceptual model and elements of a mathematical model for these effects. The DOE has implemented the EPA conceptual model (40 CFR § 194.32(b), U.S. EPA 1996) to be consistent with EPA criteria and guidance; this model is described in the CRA-2004, Chapter 6.0, Section 6.4.6.2.3. Additional information on the implementation of the mining subsidence model is available in Appendix TFIELD-2014; the CCA, Appendix MASS, Attachments 15-4 and 15-7; and Wallace (Wallace 1996).

The principal parameter in this model is the range assigned to a factor by which hydraulic conductivity in the Culebra is increased (see the CCA, Appendix MASS, Attachment 15-4). As allowed in supplementary information to Part 194, it is the only parameter changed to account for the effects of mining.

Mining has been included in scenario development for the WIPP since the earliest work on this topic (U.S. DOE 1980 [pp. 9-145 through 9-148]; Hunter 1989; Marietta et al. 1989; Guzowski 1990; Tierney 1991; WIPP Performance Assessment 1991). These early scenario developments considered both solution and room-and-pillar mining. The focus was generally on effects of mining outside the disposal system. In the CCA FEPs screening, solution mining was screened out during scenario development (see Appendix SCR-2014, FEP H58 and FEP H59). The two primary effects of mining considered were (1) changes in the hydraulic conductivity of the Culebra or other units, and (2) changes in recharge as a result of surface subsidence. These mining effects were not formally incorporated into quantitative assessment of repository performance in preliminary PAs.

The inclusion of mining in PA satisfies the requirements of section 194.32(b) to consider the effects of this activity on the disposal system.

MASS-14.0 Intrusion Borehole

The intrusion borehole modeling assumptions used in the CRA-2019 PA have been updated from those used in the CRA-2014 PA, for the most part due to changes associated with the abandonment of panel closures in Panels 3, 4, 5, and 6, as well as the decision to abandon waste emplacement in Panel 9 (see description of these changes throughout Section MASS-14.0). Despite the planned operational change to abandon waste emplacement in Panel 9, waste will continue to be modeled in Panel 9 (Zeitler et al 2017). Modeled intrusions into Panel 9 will continue to be assumed to intersect waste and no additional panels are modeled to represent waste outside of the typical 10-panel representation. Continuing to model the same mass of waste as if it is located in Panel 9 results in somewhat larger DBR and spallings releases compared to the hypothetical case of the same mass being relocated to an arbitrary location further north (Zeitler et al. 2017). Zeitler et al. (2017) also showed that the potential non-conservative condition of not considering DBRs from both the empty Panel 9 and the hypothetical Panel 9 replacement is more than covered by the conservative assumptions of the panel neighbor redefinitions (see Section MASS-14.2) (i.e., the release increases due to panel reneighboring exceed the release decreases due to not considering DBRs from an empty panel). Thus, there is no need to model intrusions into open areas—i.e., areas that do not initially contain solid waste, but may contain contaminated brine at later times. For CRA-2019 PA calculations, it is considered to be appropriately conservative with respect to releases to continue to model waste within the existing Panel 9 in lieu of adding a new waste panel to the north.

The inclusion of intrusion boreholes in PA adds to the number of release pathways for radionuclides from the disposal system that have been identified for the undisturbed repository. Direct releases to the surface may occur during drilling as particulate material from cuttings, cavings, and spallings are carried to the surface. Also, dissolved An may be carried to the surface in brine during drilling. Once abandoned, the borehole presents a possible long-term pathway for fluid flow, such as might occur between a hypothetical Castile brine reservoir, the repository, and overlying units. This topic is also addressed in the CRA-2004, Chapter 6.0, Section 6.4.7, and Appendix SCR-2014 (FEP H1 and FEP H21).

MASS-14.1 Cuttings, Cavings, and Spallings Releases during Drilling

The assumptions regarding solids releases during drilling in WIPP PA have not changed since the CRA-2014 PA. The cuttings, cavings, and spallings models estimate the quantity of An released as solids directly to the surface during drilling through the repository. The releases are caused by three mechanisms: the drill bit boring through the waste (cuttings); the drilling fluid eroding the walls of the borehole (cavings); and high repository gas pressure causing solid material failure and entrainment into the drilling fluid in the wellbore (spallings). See the CRA-2004, Chapter 6.0, Section 6.4.7.1, and references to other appendices cited in that section for additional information. Stochastic uncertainty in parameters relevant to these release mechanisms is addressed in the CRA-2004, Chapter 6.0, Section 6.4.12. The conceptual model for cuttings, cavings, and spallings is discussed in three parts because of the different processes that produce the three types of releases.

Cuttings are materials removed to the surface through drilling mud by the direct mechanical action of the drill bit. The volume of waste removed to the surface is a function of the repository

height and the drill bit area. The principal parameter in the cuttings model is the diameter of the drill bit (see Kim and Feng 2019).

Cavings are materials introduced into the drilling mud by the erosive action of circulating drilling fluid on the waste in the walls of the borehole annulus. Erosion is driven solely by the shearing action of the drilling fluid (or mud) as it moves up the borehole annulus. Shearing may be caused by either laminar or turbulent flow. The principal parameters in the cavings model are the properties of the drilling mud, drilling rates, the drill string angular velocity, and the shear resistance of the waste (see MASS-14.1.2). (See Kim and Feng 2019 for details on the sampled parameters used in the cavings model, the drill string angular velocity, and the effective shear resistance to erosion.)

Spallings are solids introduced into the wellbore by the fluid pressure difference between the repository and the bottom of the wellbore. If the repository pressure is sufficiently high (more than about 12 MPa) relative to the well bottom hole pressure (about 8 MPa), the stress state in the repository may cause repository solids to fail in the vicinity of the wellbore. In turn, these solids may become entrained in the gas flowing toward the well, ultimately to be carried up to the land surface and constituting a release. The principal parameters in the spallings model are the gas pressure in the repository when it is penetrated and properties of the waste such as permeability, tensile strength, and particle diameter. Because the release associated with spalling is sensitive to gas pressure in the repository, it is strongly coupled to the BRAGFLO-calculated conditions in the repository at the time of penetration.

MASS-14.1.1 Historical Context of Cuttings, Cavings, and Spallings Models

Cuttings and cavings releases are straightforward. The analytical equations governing erosion (cavings) based on laminar and turbulent flow (Appendix PA-2019, Section PA-4.5) have been implemented in the code CUTTINGS_S. Using selected input based on assumed physical properties of the waste and other drilling parameters, this code calculates the final caved diameter of the borehole that intersects the waste.

The various approaches used for spallings up to the CCA PA are documented in the CCA, Appendix MASS, Section MASS-16.1.1. Since the CCA PA, the spallings model has been extensively revised and has changed fundamentally from an end-state erosional model to a mechanically based, coupled material failure and transport model (WIPP Performance Assessment 2003a). This model is implemented in the code DRSPALL. An implementation error in the DRSPALL code was found and corrected for the CRA-2019 PA (Kicker, Herrick, and Zeitler 2015). A discussion tracing the historical steps from the CCA erosional model to the current DRSPALL model can be found in Appendix PA-2004, Attachment MASS, Section MASS-16.1.1.

MASS-14.1.2 Waste Mechanistic Properties

Waste mechanical properties used in the CRA-2019 PA are updated to a very minor extent from those used in the CRA-2014 PA. For intrusion events considered in WIPP PA, drilling mud flowing up the borehole will apply a hydrodynamic shear stress on the borehole wall. The WIPP PA uses the parameter BOREHOLE:TAUFAIL to represent the hydrodynamic shear strength of

the waste in the numerical code CUTTINGS_S (see Appendix PA-2019, Section PA-4.5). It is officially called the "effective shear strength for erosion," but it is more commonly known as the "waste shear strength." For the CRA-2014 PA, an updated parameterization of the waste shear strength was used (Herrick et al. 2012, Herrick and Kirchner 2013). For the CRA-2019 PA, a small decrease to the lower end of the CRA-2014 PA parameter distribution was made (Zeitler 2019c).

MASS-14.1.3 Mechanistic Model for Spall

The CRA-2019 PA uses the same spallings model that has been used since the CRA-2004 PABC. However, an error in the implementation of the spallings model in the DRSPALL code was found and corrected for the CRA-2019 PA (Kicker, Herrick, and Zeitler 2015). An updated set of DRSPALL PA calculations were documented and used for the CRA-2019 PA (Kirchner, Gilkey, and Long 2015).

In the CRA-2004 PA, an approach to modeling the WIPP spallings process was developed to address peer review concerns during the original certification process (see the CCA, Chapter 9.0, Section 9.3.1.2 and Appendix PEER-2004, Section PEER-2004 3.0). Instead of focusing on the end state after penetration, as was done in the original CCA erosional model, the new model sought to capture the system behavior from just before penetration through to the end state. In doing so, many more phenomena were included in the model. Considered in this new conceptual model was unsteady, convergent gas flow from the repository toward the wellbore that caused mechanical stress and potential failure of solids near the face of the wellbore. Pressure in the cavity at the point of penetration was balanced by the mud column in the wellbore and the repository pressure.

The spall code DRSPALL (WIPP Performance Assessment 2003a) is based on a predecessor code called GASOUT (Hansen et al. 1997, Appendix C). DRSPALL has built upon GASOUT by:

1. Adding a wellbore flow model that transports mud, repository gas, and waste solids from repository level to the land surface

2. Adding a fluidized bed model that evaluates the potential for failed particulate waste to fluidize and become entrained in the wellbore flow

The wellbore flow model in DRSPALL utilizes one-dimensional geometry with a compressible, viscous, isothermal, homogeneous mixture of mud, gas, and solids. Standard mass and momentum balance, friction loss, and slurry viscosity equations are used. Wellbore flow model results were successfully verified against those from an independent commercial code for several test problems (WIPP Performance Assessment 2003b).

DRSPALL applies the fluidized bed theory to determine the mobilization of failed material to the flow stream in the wellbore. If the escaping gas velocity exceeds the minimum fluidization velocity, failed material is fluidized and entrained for transport at the land surface. If gas velocity is too low to fluidize the bedded material, the cavity size is allowed to stabilize. The spall

volumes predicted by DRSPALL are based on the following conservative assumptions for material properties and for the flow geometry within the repository:

The particle size distribution for spallings is based on a detailed analysis (Wang 1997) of data from an expert elicitation (Carlsbad Area Office Technical Assistance Contractor [CTAC] 1997). This analysis considered several limiting cases in developing a conservative distribution for mean particle size ranging from 1 millimeter to 10 cm (Hansen, Pfeifle, and Lord 2003).

The shape factor for fluidization of particles has a potential range from 0 to 1.0. Smaller values of the shape factor denote particles that are less spherical, and therefore more easily fluidized and transported in the flow. The shape factor is conservatively set to a value of 0.1 (Lord 2003).

The tensile strength of the waste assigned for the spalling process is uncertain, ranging from 0.12 MPa to 0.17 MPa (Hansen, Pfeifle, and Lord 2003). Tensile strength data were measured in laboratory experiments on surrogate materials chosen to conservatively represent highly degraded residuals from typical wastes. The given range is felt to represent extreme, low-end tensile strengths because it does not account for several strengthening mechanisms, such as MgO hydration and halite precipitation/cementation (Hansen et al. 1997).

DRSPALL uses a hemispherical geometry (one-dimensional spherical symmetry) for the flow field and cavity in the waste. This conceptual model is appropriate when the drill bit first penetrates the repository. But, as the drill bit passes completely through the compacted waste, the flow field transitions toward a cylindrically symmetric geometry. This transition is important because the largest spall release volumes are predicted to occur at late times, well after the drill bit has penetrated through the waste, and because the spall volumes predicted for a cylindrical geometry are less than for the hemispherical geometry (Lord, Rudeen, and Hansen 2003).

In summary, the conservative assumptions for waste properties, the waste flow geometry, and the driller's actions provide very conservative spalling release volumes (see also Appendix PA-2019, Section PA-4.6 for a description of the spallings model, and Appendix PEER-2004, Section PEER-2004 3.0 for the results of the spallings model peer review). As stated previously, the DRSPALL calculations from the corrected code were used in the CRA-2019 PA (see Appendix PA-2019, Section PA-6.7.4 and Section PA-8.5.2).

MASS-14.1.4 Calculation of Cuttings, Cavings, and Spallings Releases

The modeling assumptions relating to the calculations of cuttings, cavings and spallings releases have not changed since the CRA-2014 PA. As detailed in Appendix PA-2019, Section PA-6.7.5, cuttings and cavings releases for intrusions into CH-TRU waste are computed by multiplying the volume released (calculated by the code CUTTINGS_S) by the average radioactivity concentration from three independently selected waste streams, consistent with the conceptual assumption that waste streams are randomly emplaced in waste stacks that are three drums high (note that the radioactivity concentration is scaled from the input value by the REFCON:FVW parameter, the fraction of repository volume assumed to be occupied by waste). Cuttings and cavings releases for RH-TRU waste are calculated in a similar manner to CH-TRU waste, with the exception that a single waste stream is selected, consistent with the assumption that RH-TRU waste is randomly emplaced in a manner such that a single waste canister is encountered by a

hypothetical drilling intrusion. The probability that an intrusion that intersects waste intersects CH-TRU or RH-TRU waste is based on the area parameters associated with CH-TRU and RH-TRU waste (parameters REFCON:AREA_CH and REFCON:AREA_RH; see Kim and Feng 2019).

The effect of this random emplacement assumption on PA results was examined in a separate PA (Hansen et al. 2003) in which cuttings and cavings releases were computed by assuming that each intrusion encounters only a single waste stream. The differences in repository performance (determined by comparing the mean CCDFs for releases) were determined to be minor. For more details on the analysis, see Appendix PA-2004, Attachment MASS, Section MASS-21.0.

Because spallings may release a relatively large volume of material (exceeding 4 m^3), spalling releases for intrusions into CH-TRU waste are computed by multiplying the volume of spalled material with the average CH-TRU waste concentration of radioactivity in the repository at the time of the intrusion. A separate PA (Hansen et al. 2003) compared spalling releases computed using the average concentration of radioactivity in the waste to spalling releases computed using the radioactivity of a single, randomly selected waste stream. The analysis determined that the assumption had only a minor effect on the mean CCDF for releases. For more details on the analysis, see Appendix PA-2004, Attachment MASS, Section MASS-21.0. During their completeness review of the CRA-2004, the EPA requested additional DRSPALL vectors be used in the CRA-2004 PABC. Minor changes were made to the implementation of spallings results that did not change the overall modeling assumptions. These implementation changes are outlined in Leigh et al. (Leigh et al. 2005, Section 7.8).

MASS-14.2 Direct Brine Releases during Drilling

The DBR modeling assumptions used in the CRA-2019 PA were changed from those used in the CRA-2014 PA. Material properties in some panel closure areas have changed and panel neighbor relationships associated with DBRs have also changed (changes described below). This model provides a series of calculations to estimate the quantity of brine released directly to the surface during drilling. DBRs may occur when a driller penetrates the WIPP and unknowingly brings contaminated brine to the surface during drilling (these releases are not accounted for in the cuttings, cavings, and spallings calculations, which model only the solids removed during drilling). Appendix PA-2019, Section PA-4.7, describes the DBR model used for the CRA-2019 PA. The CCA, Appendix MASS, Attachment 16-2 describes the DBR model used for the CCA PA. The conceptual model for DBRs is discussed in Appendix PA-2019, Section PA-4.7, and the CRA-2004, Chapter 6.0, Section 6.4.7.1.1.

Uncertainty in the BRAGFLO DBR calculations is captured in the 10,000-year BRAGFLO calculations from which the initial and boundary conditions are derived. BRAGFLO DBR calculations are performed for three intrusion points (designated “lower,” “middle,” and “upper” intrusions) in the waste areas corresponding to subsequent intrusions in the “same,” “adjacent,” and “non-adjacent” panels, respectively (Figure MASS-12). The model parameters that have the most influence on DBRs are repository pressure and brine saturation at the time of intrusion. Brine saturation is influenced by many factors, including Salado and MB permeability and gas-generation rates (for undisturbed scenario calculations). For E1 and E2 intrusion scenarios, Castile brine-reservoir pressure and volume, and abandoned borehole permeabilities influence

conditions for the second and subsequent intrusions. The dip in the repository (hence the location of intrusions), two-phase flow parameters (residual brine and gas saturation), time of intrusion, and duration of flow have lesser impacts on brine releases.

The implementation of the DBR model was slightly adjusted in the CRA-2014 PA to incorporate the ROMPCS. The Option D panel closure modeled in the CRA-2009 PABC was 40 m long whereas the ROMPCS modeled in the CRA-2014 PA was 30.48 m (100 ft) long. As a result, grid cell lengths corresponding to single panel closures were reduced to 30.48 m in the CRA-2014 PA. In the CRA-2019 PA, the grid lengths were maintained, but open panel closure area properties were applied to the BRAGFLO DBR grid (Figure MASS-12 and Figure MASS-13) cells associated with panel closure representations for Panels 3, 4, 5, and 6, consistent with the treatment of the southernmost panel closure in the BRAGFLO Salado grid (Figure MASS-1).

The ROMPCS, which is modeled as run-of-mine salt in the CRA-2019 PA, has no concrete component that is “keyed in” to the surrounding DRZ. As a result, material elements corresponding to equivalent DRZ/concrete in the CRA-2009 PABC were replaced by DRZ in the CRA-2014 PA and maintained for the CRA-2019 PA. Figure MASS-12 shows the DBR grid and material map used in the CRA-2019 PA. (Note that the color scheme in Figure MASS-12 is chosen to match the color scheme of the CRA-2019 BRAGFLO grid shown in Figure MASS-1.) The CRA-2009 PA used a DBR maximum duration of 4.5 days, based on current drilling practices (Appendix PA-2019, Section PA-4.7.8) and this duration remains in use in the CRA-2019 PA.

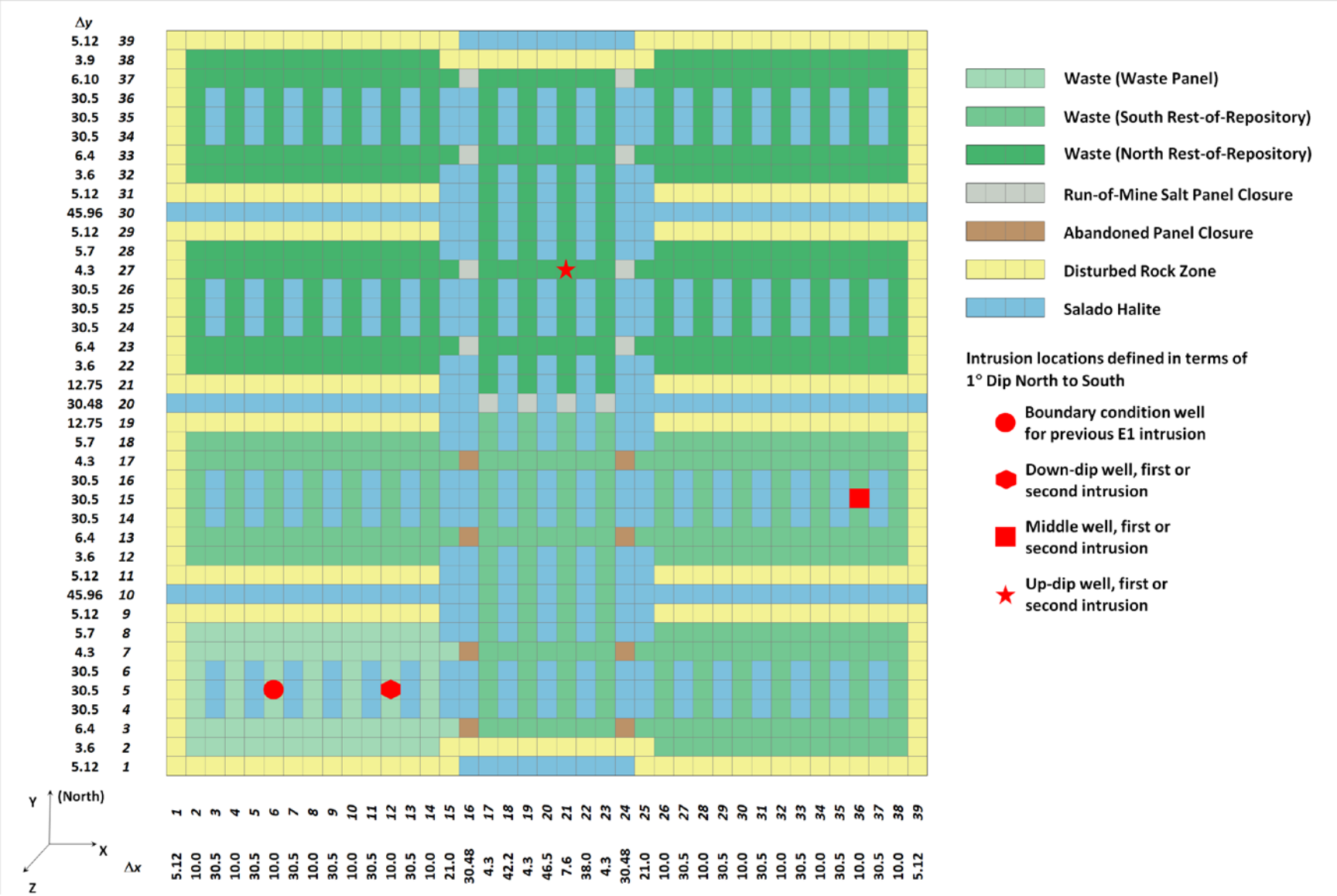

Figure MASS-12. CRA-2019 PA BRAGFLO Grid and Modeled Area Descriptions for DBR Calculations

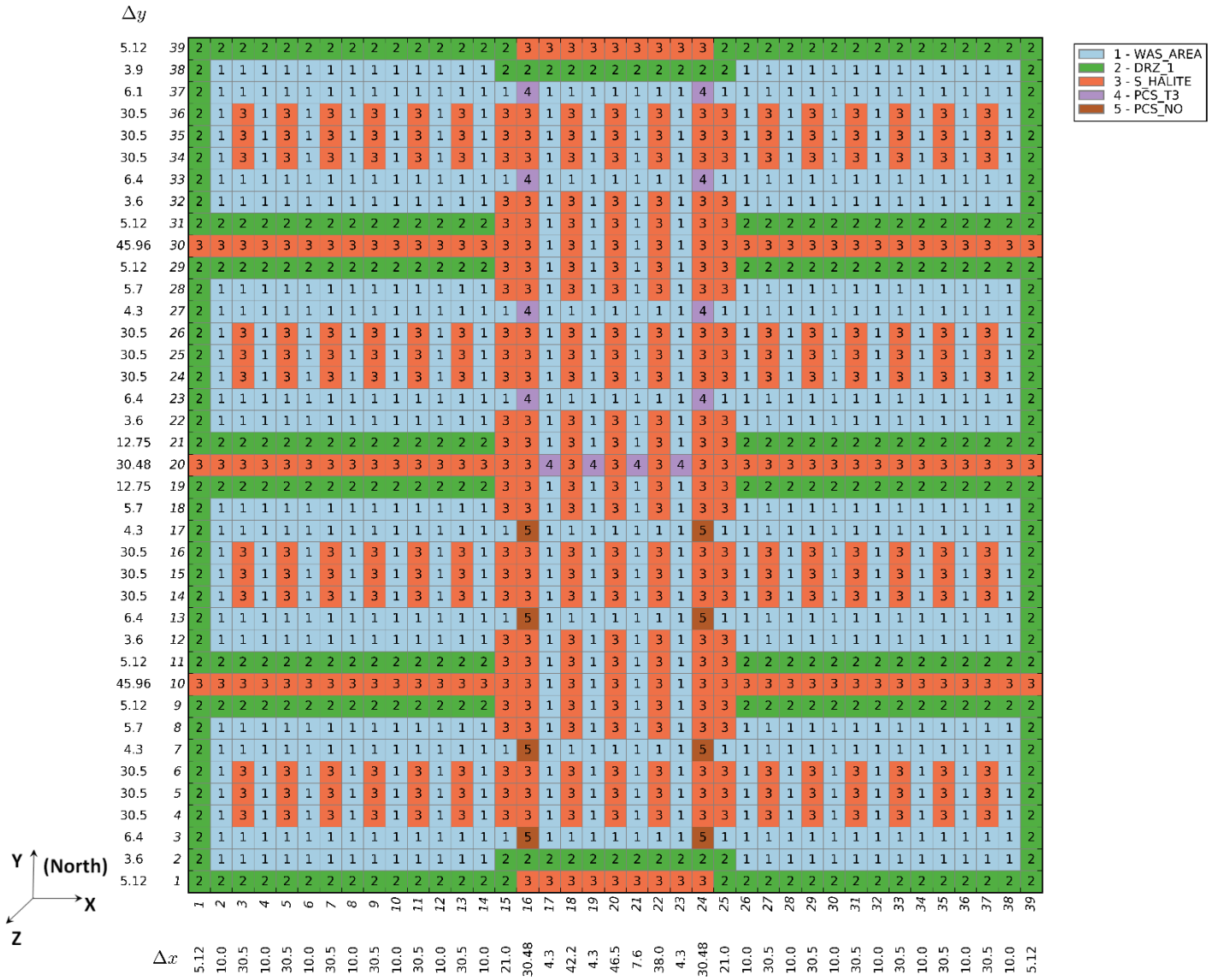

Figure MASS-13. CRA-2019 PA BRAGFLO Grid and Material Map Used for DBR Calculations

A change has been made for the CRA-2019 PA in how panel neighbor relationships are defined in CCDFGF calculations, which impacts how BRAGFLO DBR calculations are used in release calculations. The reassignment of neighbors was done for consistency with the modified repository configuration (i.e., lack of emplaced panel closures in Panels 3, 4, 5, and 6) (Zeitler et al. 2017) and is summarized in Table MASS-4.

Version 6.02 (and previous versions) of the CCDFGF code specified 144 model node locations for drilling intrusions, which corresponded to 14 locations per panel for Panels 1-8 and 16 locations each for Panels 9 and 10 (Figure PA-11 in Appendix PA, 2014). For a given intrusion into the repository, a node was chosen at random with equal probability. Node-to-Panel correlations and "panel adjacency" (the adjacent or non-adjacent relationship between panels) were specified explicitly in the CCDFGF code (i.e., were "hard-coded"). As explained above, panel adjacency is relevant to the calculation of DBRs. The CCDFGF code version 6.0 was used in CRA-2014 PA calculations.

Table MASS-4. Listing of Adjacent Panel ("Neighbor") Relationships for CRA-2014 and CRA-2019 PAs

Panel	CRA-2014_PA	CRA-2019 PA
1	2, 10	10
2	1, 3, 10	10
3	2, 4, 9	4, 5, 6, 9, 10
4	3, 9	3, 5, 6, 9, 10
5	6, 9	3, 4, 6, 9, 10
6	5, 7, 9	3, 4, 5, 9, 10
7	6, 8, 10	10
8	7, 10	10
9	3, 4, 5, 6, 10	3, 4, 5, 6, 10
10	1, 2, 7, 8, 9	1, 2, 3, 4, 5, 6, 7, 8, 9

Beginning with CCDFGF v. 7.00, the use of 144 node locations for intrusions was replaced with the use of 10 node locations (each corresponding directly to a specific panel), with node probabilities specified at run-time via relative panel areas in the CCDFGF control file (WIPP PA, 2010).[3] Panel adjacency is handled by specifying immediate (i.e., adjacent) neighbors for each panel in the CCDFGF control file. The CCDFGF v. 7.02 code was used for CRA-2019 PA calculations.

[3] As part of the process for migrating WIPP PA codes from the Alpha/VMS system to the Solaris system, the use of CCDFGF v. 7.02 was regression tested against CRA-2014 calculations with panel probabilities given as the fraction of node locations; i.e., 14/144=0.09722222 for Panels 1-8 and 16/144=0.11111111 for each of Panels 9 and 10. Panel adjacency was specified in input control files to correspond exactly to that which had been "hard-coded" in v. 6.02 (and previous versions) of CCDFGF.

The definition of panel adjacency used in the CRA-2014 PA is shown in Table MASS-4. For example, Panel 1 had Panels 2 and 10 as neighbors and Panel 5 has Panels 6 and 9 as neighbors. In the CRA-2019 PA, panel neighbor relationships were modified to correspond to the degree of separation by panel closures (Table MASS-4) instead of merely spatial proximity.[4] The modification is consistent with the definition that panels having one or fewer panel closures between them are considered neighbors. The approach is consistent with the use of panel closures in both the BRAGFLO and BRAGFLO_DBR grids and the definitions of SROR and NROR (see Figure MASS-1 and Figure MASS-12).

The neighbor relationship updates manifest themselves in two ways: (1) decreased number of neighbors for Panels 1-8 due to no longer counting adjacencies across pure halite; and (2) increased number of neighbors for panels in WP and SROR due to the reduced use of panel closures (and thus increased transmissivity between panels). Panels that are separated from each other by a single set of panel closures are considered neighbors ("Adjacent"). As an example of the first type of update, Panel 1 now only has one neighbor, Panel 10 (but not Panel 2). As an example of the second type of update, Panel 5 is now neighbors with Panels 3, 4, 6, 9, and 10. There is only a single set of panel closures between any of the WP or SROR panels and Panel 10; as a result, all other panels are neighbors of Panel 10.

As a logical extension of the updated panel neighbor relationships, the question may arise as to whether the WP and SROR areas should be modeled as a single, combined panel. That would entail, for CCDFGF calculations, treating successive intrusion into any two of Panels 3, 4, 5, 6 and 9 as the "Same" instead of "Adjacent." For this analysis, panels were not combined in order to preserve flexibility in the model because there exists uncertainty in the evolution of the "open areas" where panel closures were previously planned to be inserted. On one hand, if the open areas close relatively quickly and compact tightly (such that they behave as run-of-mine salt panel closures), then the true neighbor adjacency of those panels will have properly been preserved.[5] If, on the other hand, the open areas close slowly and compact loosely (such that they provide little barrier to brine and gas flow), then results from the "Same" and "Adjacent" BRAGFLO DBR cases will be similar because, in the BRAGFLO DBR simulations, Panels 3, 4, 5, 6 and 9 will behave as a single, large panel. Thus, in the CCDFGF calculations, any selected "Adjacent" case uses DBR results that include the effects of a lack of panel closures. Furthermore, regardless of whether there is zero or one set of panel closures between neighboring panels, CCDFGF uses the same DBR results that include the effects of a lack of panel closures. Therefore, CCDFGF calculates DBR releases that are conservative with respect to the proposed change in panel closure configurations.

MASS-14.3 Long-Term Properties of the Abandoned Intrusion Borehole

The long-term treatment and assumptions used to represent boreholes in the CRA-2019 PA remain unchanged from those used in the CRA-2014 PA. See Appendix PA-2004, Attachment

[4] For the CRA-2019 PA, actual panel areas (rather than fraction of node locations) were used to calculate panel probabilities (Schreiber, 1991); i.e., panel probabilities were 0.10439087 for Panels 1-8, 0.07910030 for Panel 9, and 0.08577271 for Panel 10.

[5] In this case, some of the neighbor designations (e.g., Panels 5 and 9) would no longer be consistent with the updated definition of panel adjacency. However, the result can be considered conservative with respect to releases, since "Adjacent" DBR results would be used in place of "Non-Adjacent" DBR results.

MASS, Section MASS-16.3, and Appendix PA-2019, Section 4.2.9, for the borehole modeling assumptions used in the CRA-2019 PA.

MASS-15.0 Climate Change

The purpose of this model is to allow quantitative consideration of the extent to which uncertainty about future climate may contribute to uncertainty in estimates of cumulative radionuclide releases from the disposal system. This model has not changed since the CRA-2014 PA. Consideration is limited to conditions that could result from reasonably possible natural climatic changes. The model is not intended to provide a quantitative prediction of future climate, nor is it intended to address uncertainty in system properties other than estimated cumulative radionuclide releases that may be affected by climate change. See Appendix PA-2004, Attachment MASS, Section MASS-17.0, and Section MASS-17.1 for current and historical information on the climate change model. The implementation of this model in PA is also discussed in the CRA-2004, Chapter 6.0, Section 6.4.9 and Appendix PA-2004, Section PA-2.1.4.6. See also the CCA, Appendix CLI for information on expected climate variability over the 10,000-year regulatory time period.

MASS-16.0 Castile Brine Reservoir

The representation of the Castile brine reservoir in BRAGFLO in the CRA-2019 PA has not changed from the CRA-2014 PA. The conceptual model for the hypothetical brine reservoir is included in PA to estimate the extent to which uncertainty about the existence of a brine reservoir under the waste disposal region may contribute to uncertainty in the estimate of cumulative radionuclide releases from the disposal system. The conceptual model is not intended to provide a realistic approximation of an actual brine reservoir under the waste disposal region. Data are insufficient to determine whether such a brine reservoir exists.

The Castile Formation is treated as an impermeable unit in PA and plays no role in the analysis except to separate the Salado from the modeled brine reservoir in the BRAGFLO grid (Figure MASS-1). In human-intrusion scenarios, the hypothetical brine reservoir can be penetrated by an intrusion borehole connecting it to the repository. The amount of brine that can enter the repository from the brine reservoir is important to PA because brine is required for gas-generation reactions and can transport radionuclides in solution, contributing to potential releases.

The properties of the hypothetical brine reservoir defined for PA include permeability, porosity, pore volume, initial pressure, and various two-phase flow parameters. Values assigned for these properties were chosen to either be consistent with the available data from and analyses of borehole penetrations of brine reservoirs in the region or to provide a reasonable response in the BRAGFLO model.

The current treatment of the brine reservoir is based on the CCA PAVT (U.S. EPA 1998) implementation in which parameter ranges for bulk compressibility and total pore volume were updated. An implementation of the constant productivity ratio approach was made for the CRA-2004 PA and the results of that implementation continue to be used. See Appendix PA-2019, Section PA-4.2.10 for the details on the implementation in this PA.

Basic geologic information about the Castile is given in the CRA-2004, Chapter 2.0, Section 2.1.3.3. The hydrology of the known brine reservoirs is discussed in the CRA-2004, Chapter 2.0, Section 2.2.1.2.2. The treatment of the hypothetical brine reservoir in PA is discussed in the CRA-2004, Chapter 6.0, Section 6.4.8.

See the CCA, Appendix MASS, Attachment 18.1 for historical information on the Castile brine reservoir model.

MASS-17.0 Clay Seam G Modeling Assumptions

The modeling assumptions used to represent Clay Seam G are described in Appendix PA-2004, Attachment MASS, Section MASS-20.0. No changes were made to these assumptions since the CRA-2004 PA. These assumptions have also been used in the CRA-2019 PA.

MASS-18.0 Evaluation of Waste Structural Impacts, Emplacement, and Homogeneity

During the development of the CCA PA, the DOE chose to assume random placement of TRU waste in the WIPP and developed conceptual and numerical models accordingly. The EPA reviewed these models and their results and determined that the DOE had adequately modeled random placement of waste in the disposal system. The CCA PA also assumed that all waste could be modeled as if the waste was emplaced in 55-gallon drums. In accordance with the requirements of 40 CFR § 194.24(d) (U.S. EPA 2004), all PAs have assumed that waste is emplaced in a random or homogeneous manner. The PAs executed in support of compliance applications have not specifically accounted for heterogeneity in waste materials or in waste containers. Details of previous investigation into this assumption are found in MASS-2014, Section MASS-19.0. For CRA-2019 the assumption of random emplacement is used.

MASS-19.0 References

(*Indicates a reference that has not been previously submitted.)

Bear, J. 1972. Dynamics of Fluid in Porous Media. New York: Elsevier.

Camphouse, R.C., D.C. Kicker, S. Kim, T.B. Kirchner, J.J. Long, B.N. Malama, and T.R. Zeitler. 2013. Summary Report of the 2014 Compliance Recertification Application Performance Assessment. Carlsbad, NM: Sandia National Laboratories. ERMS 560252.*

Carlsbad Area Office Technical Assistance Contractor (CTAC). 1997. Expert Elicitation on WIPP Waste Particle Diameter Size Distribution(s) During the 10,000-Year Regulatory Post-Closure Period (Final Report, June 3). Carlsbad, NM: U.S. Department of Energy. ERMS 541365.

Christian-Frear, T.L., and S.W. Webb. 1996. The Effect of Explicit Representation of the Stratigraphy on Brine and Gas Flow at the Waste Isolation Pilot Plant. Albuquerque, NM: Sandia National Laboratories. SAND94-3173 WPO 37240.

Clayton, D.J., S. Dunagan, J.W. Garner, A.E. Ismail, T.B. Kirchner, G.R. Kirkes, and M.B. Nemer. 2008. Summary Report of the 2009 Compliance Recertification Application Performance Assessment. Carlsbad, NM: Sandia National Laboratories. ERMS 548862.

Clayton, D.J., R.C. Camphouse, J.W. Garner, A.E. Ismail, T.B. Kirchner, K.L. Kuhlman, M.B. Nemer. 2010. Summary Report of the CRA-2009 Performance Assessment Baseline Calculation. Carlsbad, NM: Sandia National Laboratories. ERMS 553039.

Cotsworth, E. 2005. Letter to I. Triay (Subject: EPA Letter on Conducting the Performance Assessment Baseline Change (PABC) Verification Test). 4 March 2005. U.S. Environmental Protection Agency, Office of Air and Radiation, Washington, DC. ERMS 538858.

Cotsworth, E. 2009. Letter to D. Moody (Subject: EPA CRA-2009 First Set of Completeness Comments). 21 May 2009. U.S. Environmental Protection Agency, Office of Air and Radiation Washington, DC. ERMS 551444.

Davies, P.B. 1991. Evaluation of the Role of Threshold Pressure in Controlling Flow of Waste-Generated Gas into Bedded Salt at the Waste Isolation Pilot Plant. Albuquerque, NM: Sandia National Laboratories. SAND90-3246. WPO 26169.

Davies, P.B., S.W. Webb, and E.D. Gorham. 1992. Memorandum to B.M. Butcher, J. Schreiber, and P. Vaughn (Subject: Feedback on “PA Modeling Using BRAGFLO -- 1992” 7-8-92 memo by J. Schreiber; 4 Attachments). (July 14, 1992). Albuquerque, NM: Sandia National Laboratories.

Day, B. 2019. Reassessment of Need and Parameter Justification for Modeling Gas Generation due to Radiolysis of Brine and Cellulose/Plastic/Rubber in WIPP for CRA-2019. Carlsbad, NM: Sandia National Laboratories. ERMS 570873.*

Freeze, G.A., K.W. Larson, and P.B. Davies. 1995. Coupled Multiphase Flow and Closure Analysis of Repository Response to Waste-Generated Gas at the Waste Isolation Pilot Plant (WIPP). Albuquerque, NM: Sandia National Laboratories. SAND93-1986, ERMS 229557.

Gorham, E., R. Beauheim, P. Davies, S. Howarth, and S. Webb. 1992. Recommendations to PA on Salado Formation Intrinsic Permeability and Pore Pressure for 40 CFR 191 Subpart B Calculations, June 15, 1992. Preliminary Performance Assessment for the Waste Isolation Pilot Plant, December 1992 Volume 1, pp. A-49 - A-65. Albuquerque, NM: Sandia National Laboratories. SAND92-0700/3.

Guzowski, R.V. 1990. Preliminary Identification of Scenarios for the Waste Isolation Pilot Plant, Southeastern New Mexico. Albuquerque, NM: Sandia National Laboratories. SAND90-7090. WPO 25771.

Hansen, F.D., M.K. Knowles, T.W. Thompson, M. Gross, J.D. McLennan and J.F. Schatz. 1997. Description and Evaluation of a Mechanically Based Conceptual Model for Spall. Albuquerque, NM: Sandia National Laboratories. SAND97-1369.

Hansen, C.W., L.H. Brush, M.B. Gross, F.D. Hansen, B. Park, J.S. Stein, and T.W. Thompson. 2003. Effects of Supercompacted Waste and Heterogeneous Waste Emplacement on Repository Performance (Revision 1). Carlsbad, NM: Sandia National Laboratories. ERMS 532475.

Hansen, F.D., T.W. Pfeifle, and D.L. Lord. 2003. Parameter Justification Report for DRSPALL (Revision 0). Carlsbad, NM: Sandia National Laboratories. SAND2003-2930.

Herrick, C.G., M.D. Schuhen, D.M. Chapin, and D.C. Kicker. 2012. Determining the Hydrodynamic Shear Strength of Surrogate Degraded TRU Waste Materials as an Estimate for the Lower Limit of the Performance Assessment Parameter TAUFAIL. Carlsbad, NM: Sandia National Laboratories. ERMS 558479.

Herrick, C.G., and T. Kirchner 2013. Memorandum to C Camphouse (Subject: Follow-up to Questions Concerning TAUFAIL Flume Testing Raised during the November 14-15, 2012 Technical Exchange Between the DOE and EPA). (January 23, 2013). Carlsbad, NM: Sandia National Laboratories. ERMS 559081.

Hunter, R.L. 1989. Events and Processes for Constructing Scenarios for the Release of Transuranic Waste from the Waste Isolation Pilot Plant, Southeastern New Mexico. Albuquerque, NM: Sandia National Laboratories. SAND89-2546. WPO 27731.

Kicker, D.C., C. Herrick, and T. Zeitler. 2015. Impact of the DRSPALL Modification on Waste Isolation Pilot Plant Performance Assessment Calculations. Carlsbad, NM: Sandia National Laboratories. ERMS 564863. *

Kicker, D.C. 2019. Radionuclide Inventory Screening Analysis Report for the 2019 Compliance Recertification Application Performance Assessment, Rev. 1. Carlsbad, NM: Sandia National Laboratories. ERMS 571659. *

Kim, S. and L. Feng. 2019. Parameter Summary Report for the 2019 Compliance Recertification Application, Rev. 1. Carlsbad, NM: Sandia National Laboratories. ERMS 571660. *

Kirchner, T., A. Gilkey, and J. Long. 2015. Addendum to the Summary Report on the Migration of the WIPP PA Codes from VMS to Solaris, AP-162. Carlsbad, NM: Sandia National Laboratories. ERMS 564675. *

Leigh, C., J. Kanney, L. Brush, J. Garner, G. Kirkes, T. Lowery, M. Nemer, J. Stein, E. Vugrin, S. Wagner, and T. Kirchner. 2005. 2004 Compliance Recertification Application Baseline Performance Assessment Calculation (Revision 0). Carlsbad, NM: Sandia National Laboratories. ERMS 541521.

Lord, D.L. 2003. Justification for Particle Diameter and Shape Factor used in DRSPALL. Carlsbad, NM: Sandia National Laboratories. ERMS 531477.

Lord, D., D. Rudeen, and C. Hansen. 2003. Analysis Package for DRSPALL: Compliance Recertification Application. Part I–Calculation of Spall Volumes. Carlsbad, NM: Sandia National Laboratories. ERMS 532766.

Marietta, M.G., S.G. Bertram-Howery, D.R. Anderson, K.F. Brinster, R.V. Guzowski, H. Iuzzolino, and R.P. Rechard. 1989. Performance Assessment Methodology Demonstration: Methodology Development for Evaluating Compliance with EPA 40 CFR 191, Subpart B, for the Waste Isolation Pilot Plant. Albuquerque, NM: Sandia National Laboratories. SAND89-2027. WPO 25952.

Mendenhall, F.T., and W. Gerstle. 1993. Memorandum to Distribution (Subject: WIPP Anhydrite Fracture Modeling), (December 6, 1993). Albuquerque, NM: Sandia National Laboratories. WPO 39830. SWCF-A: W.B.S. 1.1.7.1.

Park, B., and F.D. Hansen. 2003. Analysis Report for Determination of the Porosity Surfaces of the Disposal Room Containing Various Waste Inventories for WIPP PA (Revision 0). Albuquerque, NM: Sandia National Laboratories. ERMS 533216.

Reed, D., J. Swanson, and F. Stanley. 2019. LANL/ACRSP Parameter Recommendations for the CRA-2019 Deferred Performance Assessment, Rev. 1. Los Alamos National Laboratory, Carlsbad, NM. ERMS 571296. *

Schreiber, J. 1991. Updated Waste Storage Volumes. Carlsbad, NM: Sandia National Laboratories. ERMS 237713. *

Schreiber, J.D. 1997. WIPP PA User's Manual for BRAGFLO (Version 4.10, May). Carlsbad, NM: Sandia National Laboratories. ERMS 245238.

Tierney, M.S. 1991. Combining Scenarios in a Calculation of the Overall Probability Distribution of Cumulative Releases of Radioactivity From the Waste Isolation Pilot Plant, Southeastern New Mexico. Albuquerque, NM: Sandia National Laboratories. SAND90-0838. WPO 26030.

U.S. Department of Energy (DOE). 1980. Final Environmental Impact Statement, Waste Isolation Pilot Plant (October). 2 vols. DOE/EIS-0026. Washington, DC: U.S. Department of Energy. ERMS 238835 (vol. 1) and ERMS 238838 (vol. 2).

U.S. Department of Energy (DOE). 1996. Title 40 CFR Part 191 Compliance Certification Application for the Waste Isolation Pilot Plant (October). 21 vols. DOE/CAO 1996-2184. Carlsbad, NM: Carlsbad Area Office.

U.S. Department of Energy (DOE). 2004. Title 40 CFR Part 191 Compliance Recertification Application for the Waste Isolation Pilot Plant (March). 10 vols. DOE/WIPP 2004-3231. Carlsbad, NM: Carlsbad Field Office.

U.S. Department of Energy (DOE). 2009. Title 40 CFR Part 191 Compliance Recertification Application for the Waste Isolation Pilot Plant. DOE/WIPP 09-3424. Carlsbad, NM: Carlsbad Field Office.

U.S. Department of Energy (DOE). 2014. Title 40 CFR Part 191 Compliance Recertification Application for the Waste Isolation Pilot Plant (March). Carlsbad Field Office, Carlsbad, NM. DOE/WIPP 2014-3503. *

U.S. Department of Energy (DOE). 2018. Delaware Basin Monitoring Annual Report. Carlsbad, NM: Carlsbad Field Office. DOE/WIPP-18-2308, Rev. 1. *

U.S. Environmental Protection Agency (EPA). 1996. 40 CFR Part 194: Criteria for the Certification and Recertification of the Waste Isolation Pilot Plant's Compliance with the 40 CFR Part 191 Disposal Regulations; Final Rule. Federal Register, vol. 61 (February 9, 1996): 5223–45.

U.S. Environmental Protection Agency (EPA). 1998. Technical Support Document for 194.23: Parameter Justification Report (May). Washington DC: Office of Radiation and Indoor Air.

U.S. Environmental Protection Agency (EPA). 2004. 40 CFR Part 194: Criteria for the Certification and Recertification of the Waste Isolation Pilot Plant's Compliance with the Disposal Regulations; Alternative Provisions (Final Rule). Federal Register, vol. 69 (July 16, 2004): 42571–83.

Vaughn, P., M. Lord, and R. MacKinnon. 1995a. Memorandum to D.R. Anderson (Subject: DR-6: Brine Puddling in the Repository due to Heterogeneities). (December 21, 1995). Albuquerque, NM: Sandia National Laboratories. SWCF-A:1.1.6.3. WPO 30795.

Vaughn, P., M. Lord, and R. MacKinnon. 1995b. Memorandum to D.R. Anderson (Subject: DR-7: Permeability Varying with Porosity in Closure Regions). (December 21, 1995). Albuquerque, NM: Sandia National Laboratories. SWCF-A:1.1.6.3. WPO 30796.

Vaughn, P., M. Lord, and R. MacKinnon. 1995c. Memorandum to D. R. Anderson (Subject: DR3: Dynamic Closure of the North End and Hallways). (September 28, 1995). Albuquerque, NM: Sandia National Laboratories. SWCF-A:1.1.6.3. WPO 30794.

Vaughn, P., M. Lord, and R. MacKinnon. 1995d. Memorandum to D.R. Anderson (Subject: DR-2: Capillary Action [Wicking] within the Waste Materials). (December 21, 1995). Albuquerque, NM: Sandia National Laboratories. SWCF-A:1.1.6.3. WPO 30793.

Vaughn, P., M. Lord, and R. MacKinnon. 1995e. Memorandum to D.R. Anderson (Subject: S-6: Dynamic Alteration of the DRZ/Transition Zone). (September 28, 1995). Albuquerque, NM: Sandia National Laboratories. WPO 30798.

Wallace, M. 1996. Summary Memo of Record for NS-11: Subsidence Associated with Mining Inside or Outside the Controlled Area. Records Package for Screening Effort NS-11: Subsidence Associated with Mining Inside or Outside the Controlled Area (November 21) (pp. 1–28). Albuquerque, NM: Sandia National Laboratories. ERMS 412918.

Wang, Y. 1997. Memorandum to Margaret Chu (Subject: Estimate WIPP Waste Particle Sizes on Expert Elicitation Results: Revision 1). (August 5, 1997). Albuquerque, NM: Sandia National Laboratories. ERMS 246936.

Webb, S. 1995. Memorandum to D.R. Anderson (Subject: DR-1:3D Room Flow Model with Dip). 30 May 1995. Albuquerque, NM: Sandia National Laboratories. SWCF-A:1.1.6.3. WPO 22494.

WIPP Performance Assessment. 1991. Preliminary Comparison with 40 CFR Part 191, Subpart B, for the Waste Isolation Pilot Plant. Albuquerque, NM: Sandia National Laboratories. December 1991. 4 vol. SAND91-0893/1–4.

WIPP Performance Assessment. 1993. Preliminary Performance Assessment for the Waste Isolation Pilot Plant, December 1992. Volume 4: Uncertainty and Sensitivity Analyses for 40 CFR 191, Subpart B. Albuquerque, NM: Sandia National Laboratories. SAND92-0700/4. ERMS 223528.

WIPP Performance Assessment. 2003a. Design Document for DRSPALL Version 1.00 (Version 1.10, September). Carlsbad, NM: Sandia National Laboratories. ERMS 529878.

WIPP Performance Assessment. 2003b. Verification and Validation Plan and Validation Document for DRSPALL Version 1.00 (Version 1.00, September). ERMS 524782. Carlsbad, NM: Sandia National Laboratories. ERMS 524782

WIPP PA. 2010. Design Document and User's Manual for CCDFGF (Version 7.00). Carlsbad, NM: Sandia National Laboratories. ERMS 554046.*

Zeitler, T.R, B. Day, J. Bethune, R. Sarathi, J. Long. 2017. Assessment of Abandoned Panel Closures in South End of Repository and Lack of Waste Emplacement in Panel 9 Carlsbad, NM: Sandia National Laboratories. ERMS 568459.*

Zeitler, T.R. 2018a. Cumulative Distribution for STEEL:CORRMCO2 for the CRA-2019 PA. Carlsbad, NM: Sandia National Laboratories. ERMS 570869.*

Zeitler, T.R. 2018b. Bounding Calculation of the Cumulative Distribution for STEEL:HUMCORR. Carlsbad, NM: Sandia National Laboratories. ERMS 569807.*

Zeitler, T.R. 2019a. Analysis Plan for the 2019 WIPP Compliance Recertification Application Performance Assessment. Carlsbad, NM: Sandia National Laboratories. ERMS 571150.*

Zeitler, T.R. 2019b. Calculation of Shaft and Experimental Area Dimensions for Use in the CRA-2019 PA. Carlsbad, NM: Sandia National Laboratories. ERMS 571045.*

Zeitler, T.R. 2019c. A Summary of EPA/DOE Defined Parameters to be Implemented in the CRA-2019 PA. Carlsbad, NM: Sandia National Laboratories. ERMS 570879.*

This page intentionally left blank.